as previously described (Nakazawa and Ohno, 1996; Nakazawa et al., 1998). Oocytes were bathed in ND96 solution containing (in mM) NaCl 96, KCl 2, $CaCl_2$ 1.8, $MgCl_2$ 1, HEPES 5 (pH 7.5 with NaOH) at room temperature. For the construction of concentration–response curves, ATP (adenosine 5′ -triphosphate disodium salt; Sigma, St. Louis, MO, USA) was applied by superfusion for 7 s with a regular interval of 1 min from the lowest concentration (usually 30 μM). To determine desensitization time course, ATP was applied for 30 s. For the determination of the time course of recovery from desensitization, reference responses to ATP were measured with an interval of 4 min, and trials were made with various intervals.

2.2. Data analysis

All the data were given as mean ± S.E. Curve fittings to data were made using Microsoft' Excel X. For "activation" of channels (see Fig. 2), curves were calculated from the following equation (Tallarida and Jacob, 1979):

$$E = E_{max} \cdot A^n/[A^n + (EC_{50})^n] \quad (1)$$

where E is an effect (current response), E_{max} is an maximal response, A is ATP concentration, EC_{50} is concentration required for a half-maximal effect, and n is a Hill coefficient (slope factor). As for "inactivation" curves, the following equation was used:

$$E = E_{max} \cdot (1 - A^n/[A^n + (EC_{50})^n]). \quad (2)$$

Curve fittings to the recovery from desensitization (Fig. 5) were made with an assumption of the following Hodgkin–Huxley type gating mechanism (Hille, 1992a):

$$I = m^k \cdot I_{max} \quad (3)$$

where I is current activated by ATP, I_{max} is its maximal value, k is the number of gates, and m is a gate variable given by:

$$m = 1 - \exp(-t/\tau) \quad (4)$$

where τ is a time constant.

3. Results

3.1. Concentration–response relationship

Fig. 1 shows concentration–response relationships for ATP-activated current permeating through the wild type and pore mutant $P2X_2$ receptor/channels. For the pore mutants, alanine-substituted ones were used except for D349N because D349A was an non-expressing mutant. Compared to the wild type channel, N333A and D349N exhibited higher sensitivities to ATP. Unlike the wild type channel, current responses to ATP were rather reduced at highest concentrations (300 μM, 1 mM or 3 mM) for N333A, T336A, L338A and D349N. To analyze these properties quantitatively, we plotted the relationships separately, and curve fittings were made (Fig. 2). Modeling after the gating theory for voltage-gated channels (Hodgkin and Huxley, 1952; Hille, 1992a), "activation" and "inactivation" curves were fitted to the data as described in Materials and methods. All the curves were well fitted to the data when assuming a common Hill coefficient of 2. For "activation", EC_{50} values for N333A (50 μM) and D349N (60 μM) were smaller than that for the wild type receptor (100 μM). On the other hand, a larger EC_{50} value (180 μM) was necessary for L338A activation fitting. As for "inactivation", the decease of the current responses to higher concentrations of ATP could be fitted with curves with EC_{50} values of millimolar for N333A, T336A, L338A and D349N. The results imply that the decrease can be explained if assuming that higher concentrations of ATP shut an "inactivation" gate.

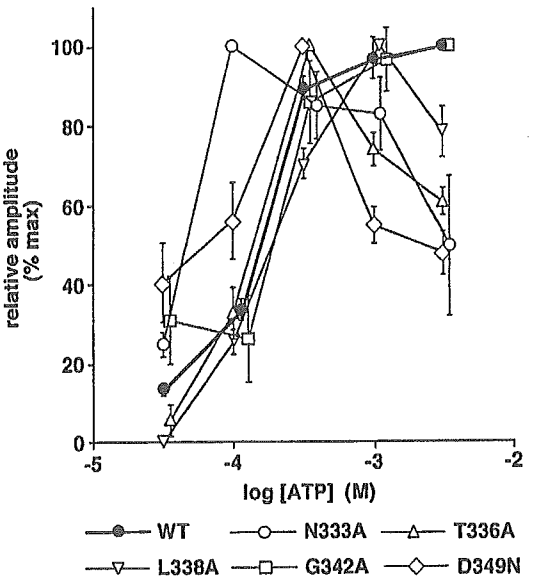

Fig. 1. Concentration–response relationships for ionic current activated by ATP permeating through the wild type (WT) and five pore mutant (N333A, T336A, L338A, G342A and D349N) channels. A current response to each concentration of ATP at − 50 mV was normalized to the maximal response in each oocyte. Each symbol represents the mean obtained four to six oocytes tested. Bars are S.E.

3.2. Desensitization time course

Fig. 3 compares time course of inward current activated by ATP for 30 s. The current permeating through the wild type channel sustained during a 30-s exposure to 1 mM ATP (Fig. 3A) whereas that through D349N markedly decayed (Fig. 3B). The results indicate that desensitization occur to D349N but not to the wild type channel. The current remaining at the end of the 30-s exposure to 100 μM or 1 mM ATP was plotted in Fig. 3C. Marked desensitization was observed with the current permeating through N333A and G342A as well as D349N. The extent of

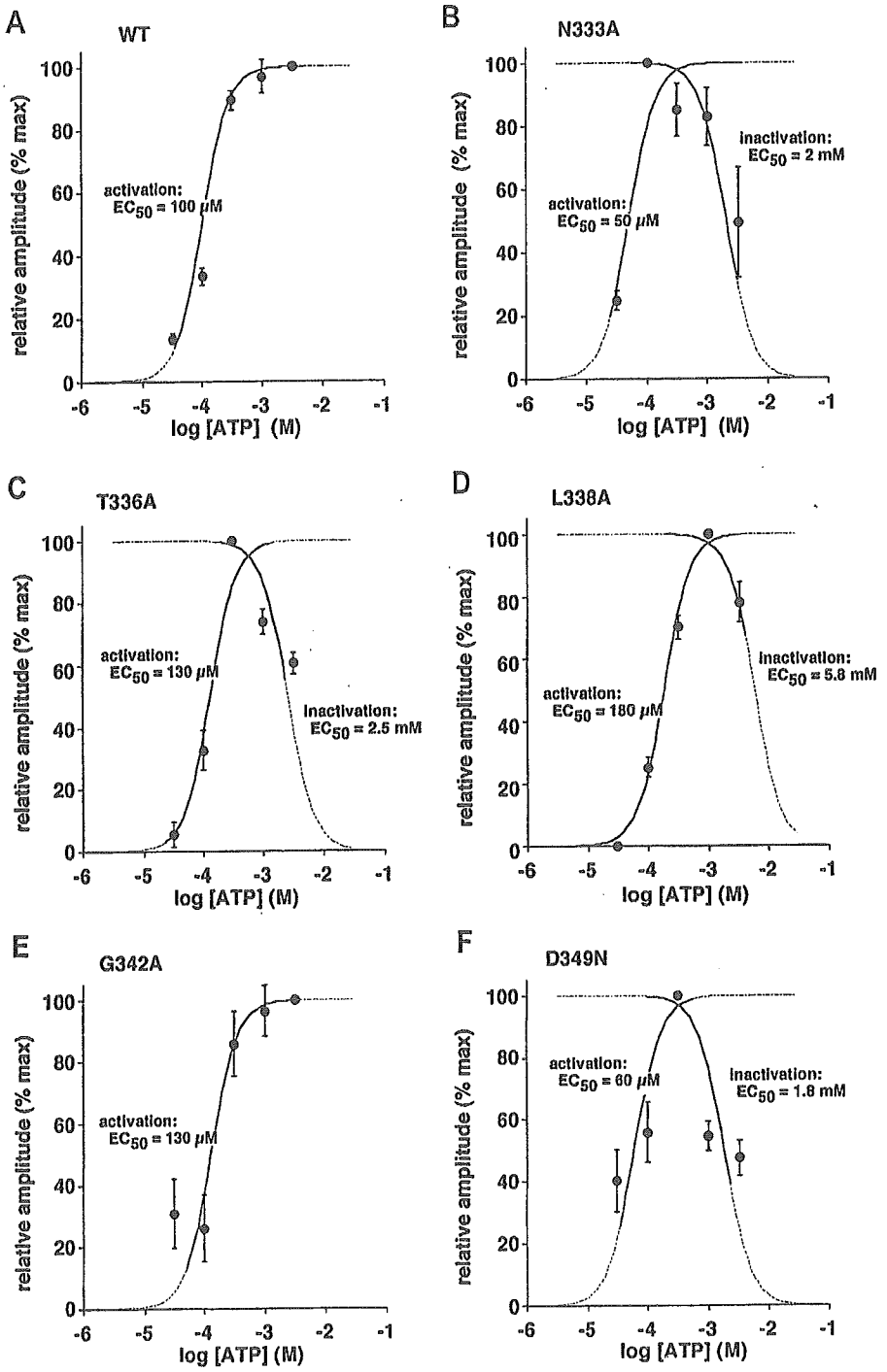

Fig. 2. Curve-fittings to concentration–response data for the ATP-activated current. "Activation" and "inactivation" curves were fitted to the data shown in Fig. 1 assuming a Hill coefficient of 2 and EC_{50} values shown in panels A to F.

desensitization was not different between the current activated by 100 μM ATP and that by 1 mM ATP for each mutant when the remaining current amplitude was compared (Fig. 3C). The current activated by a lower concentration (30 μM) of ATP was not desensitized up to 1 min for D349N (not shown).

The current amplitude remaining at the end of the 30-s exposure does not necessarily reflect desensitization time course because this value may be affected by other factors such as activation kinetics or multiple components of desenstization. Thus, the time course was further analyzed by measuring time constants. The oocytes were periodically stepped to −80 from −50 mV to obtain large current amplitude and to confirm clamp conditions of oocytes. For the current mediated through D349N shown in Fig. 3B, the decay could be fitted by a single

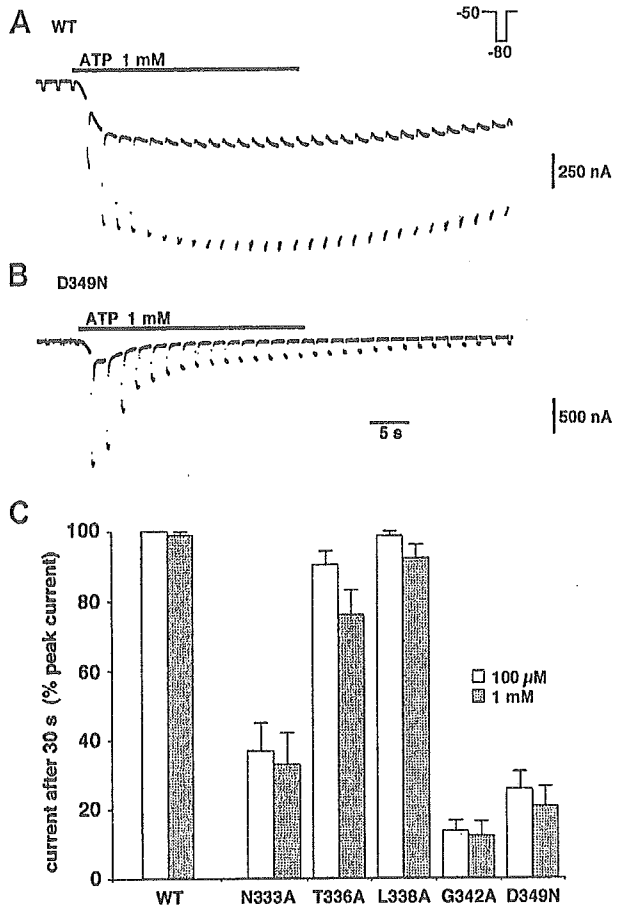

Fig. 3. Desensitization of ATP-activated current. (A, B) Comparison of time courses of ATP-activated current permeating through the wild type (WT; A) and D349N mutant (B) channels. ATP (1 mM) was applied for 30 s. The oocytes were held at − 50 mV and stepped to − 80 mV for 400 ms every 2 s. Note that the current through the wild type channel (A) was not desensitized whereas that through D349N mutant channel (B) was desensitized. (C) Comparison of the extent of desensitization. The current remaining at the end of 30 s application of 100 μM or 1 mM ATP was normalized to the peak amplitude, and plotted for the wild type (WT) and five pore mutant channels. Each column represents the mean obtained from five to seven oocytes tested. Bars are S.E.

exponential time course with a time constant of 5 s (Fig. 4A). Time constants obtained in this manner were compared in Fig. 4B. Like the current amplitude remaining at the end of the ATP exposure (Fig. 3C), the time constants were not different between the currents activated by 100 μM and 1 mM ATP for N333A and D349N. With G342A, the time constants for the current activated by 1 mM ATP were, however, smaller than that by 100 μM ATP.

3.3. Recovery from desensitization

Once desensitized, the current was not readily restored. After a 2-min washout period, the current permeating through D349N was recovered to about a half of the initial level (Fig. 5A). Fig. 5B and C shows the time course of recovery from desensitization of the currents through N333A and D349N. For both mutants, the currents were recovered to about initial levels after a 4-min washout period. For G342A, the current was recovered only to 36.1 ± 11.6% of the initial level after 4 min.

Curve fittings were made for time courses of the recovery from desensitization using the Eqs. (3) and (4) in Materials and methods. When a single "recovery" gate is assumed, the current amplitude after short washout periods (1 and 2 min) was poorly fitted by curves adjusted to fit to the current amplitude after a 4-min washout period (Fig. 5B and C; $k = 1$). This means that the initial recovery was slower than that expected from this single gate model. The fittings became better when multiple "recovery" gates are assumed (Fig. 5B and C;

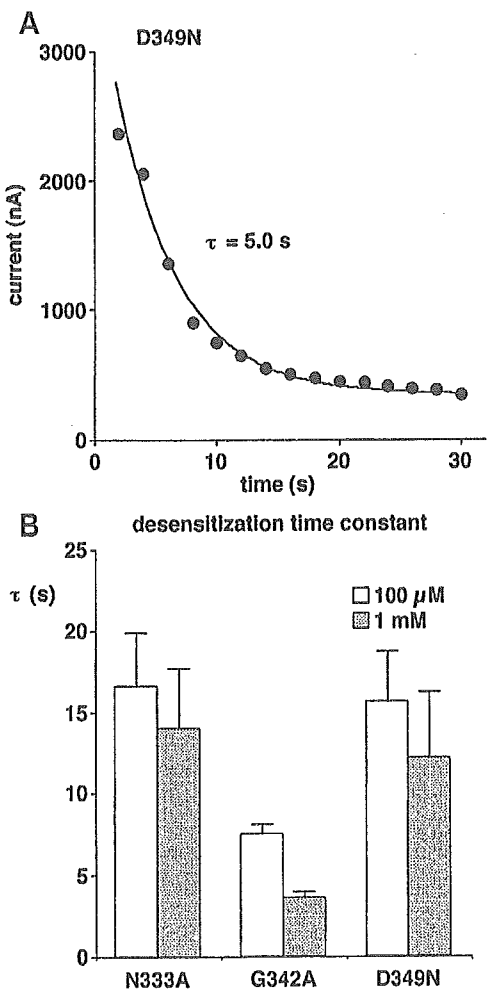

Fig. 4. Desensitization time constants. (A) A curve-fitting to the desensitization time course of ATP-activated current permeating through D349 mutant channel. The data were obtained from the current trace shown in Fig. 3B. The current amplitude at − 80 mV was plotted against the time after the beginning of the ATP-application. The data were well fitted with a single exponential time course with a time constant of 5.0 s. (B) Desensitization time constants for three pore mutants. The time constants were obtained as illustrated in A. Each column represents the mean obtained from five to seven oocytes tested. Bars are S.E.

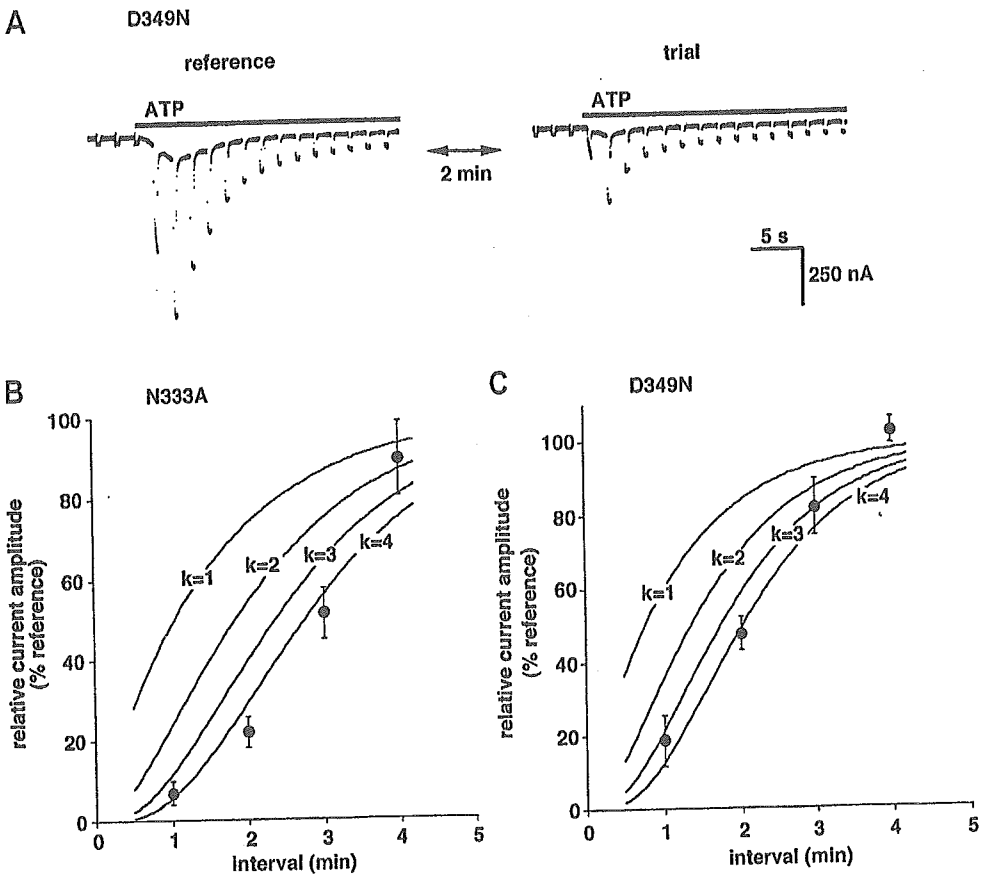

Fig. 5. Recovery from desensitization. (A) Current responses to two sequential 30-s applications of 1 mM ATP with an interval of 2 min in a D349N expressing oocyte. The response to the second application (trial) was about 40% of that to the first application (reference) in this case. (B) Time courses of recovery from desensitization of the current permeating through N333A (B) and D349N (C). Each symbol represents the mean from six oocytes tested. Bars are S.E.M. Three curves in each panel are curve-fittings with assumption of one, two, three and four homogeneous gates with a time constant of 1.5 min (N333A) or 1.1 min (D349N), respectively.

$k=2$, 3 and 4) because these multiple gate models allow slower initial recovery.

4. Discussion

In the present study, we first analyzed the "inactivation-like" property observed in the concentration–response relationship for the mutants of $P2X_2$ receptor/channel, and then analyzed the desensitization process of the mutants to compare the desensitization with the "inactivation". The mutants used in the present study possess amino acid substitutions at TM2 region of $P2X_2$ receptor/channel. This region contributes to the forming of the channel pore, and N333, T336, L338, G342 and D349 face the aqueous phase in the pore (Rassendren et al., 1997; Egan et al., 1998). The binding-site for ATP molecules are believed to be somewhere in the extracellular region of P2X receptor involving basic residues near the outer mouth of the channel pore (Ennion et al., 2000; Jiang et al., 2000). Thus, the changes in sensitivity to ATP (Fig. 1) or kinetics (Fig. 3) may not be due to direct influence by the amino acid substitutions of ATP binding, but due to some allosteric influence.

N333A, T336A, L338A and D349N exhibited reduced responses to higher concentrations of ATP (Fig. 2). These "downward limbs" could be fitted with "inactivation" curves with EC_{50} values of millimolar order. This fact may not imply the appearance of a second low-affinity binding-site on receptor subunits with these mutations. Rather, this fact may imply that the induction of this "inactivation-like" site requires higher energy than that necessary for the open state, and, thus, larger occupation by ATP molecules of the receptors is necessary. This is explained by the following simple sequential scheme (Tallarida and Jacob, 1979): where R is a receptor and A is an

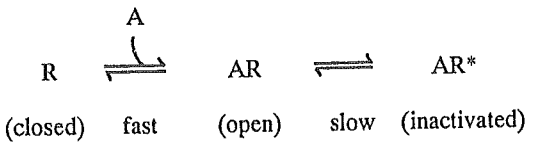

Scheme 1.

agonist (ATP). In this scheme, only one ATP molecule and one receptor subunit are shown for simplicity. The number of inactivated receptors (AR*) is negligible when the concentration of ATP is low. The number of AR* becomes considerable only when the concentration of ATP is high and as, a result, the number of AR is large.

If the process toward the inactivated state in Scheme 1 is slow enough, the current amplitude does not readily reach its steady-state, and this process will be observed as a current decay during a long exposure to ATP. In fact, the currents permeating through N333A and D349N, which exhibited "inactivation" in the concentration–response relationships (Fig. 2B and F), decayed during a 30-s exposure to high concentrations of ATP (Fig. 3B, C) whereas the current through the wild type channel did not exhibit such decay (Fig. 3A, C). However, this is not the case with the remaining pore mutants, T336A, L338A and G342A. T336A and L338A exhibited "inactivation" in the concentration–response relationships (Fig. 2C and D), but the current permeating through these mutants did not remarkably decay (Fig. 3C). As for G342A, the "inactivation" was not observed in the concentration–response relationship (Fig. 2E), the current through this mutant markedly decayed (Fig. 2C). The discrepancy may be explained if another "desensitized" state is added to the Scheme 1: (Scheme 2).

According to this scheme, "inactivation" and "desensitization" are independent processes. The transition to the inactivated state (AR*) is slow but faster than the transition to the desensitized state (AR**). AR and AR* readily reach their equilibrium, and the portion of the inactivated channels is observed as a reduction in peak amplitude, but not as a decay in current amplitude with time. In contrast, AR and

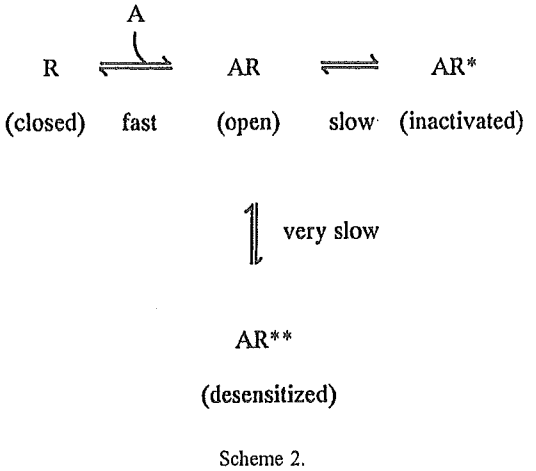

Scheme 2.

AR** do not readily reach their equilibrium, and the transition to AR** is observed mainly as a current decay with time after peak current. The transition to AR** may be slower enough for the current decay to be independent of agonist concentrations (Fig. 3). N333A and D349N can shift into both AR* and AR**, T336A and L338A can shift mainly into AR*, G342A can shift only into AR**, and the wild type channel can shift into neither AR* nor AR**. Further study will be necessary whether or not the proposed two states can be defined as molecular conformations of the receptor.

The desensitization time course of N333A, G342A and D349N could be fitted by a single exponential (Fig. 4). This suggests that the closing of a single gate is sufficient to induce the desensitization. On the other hand, the time course of the recovery from the desensitization was not well fitted by a single exponential, and the introduction of multiple exponentials resulted in better fittings to the data

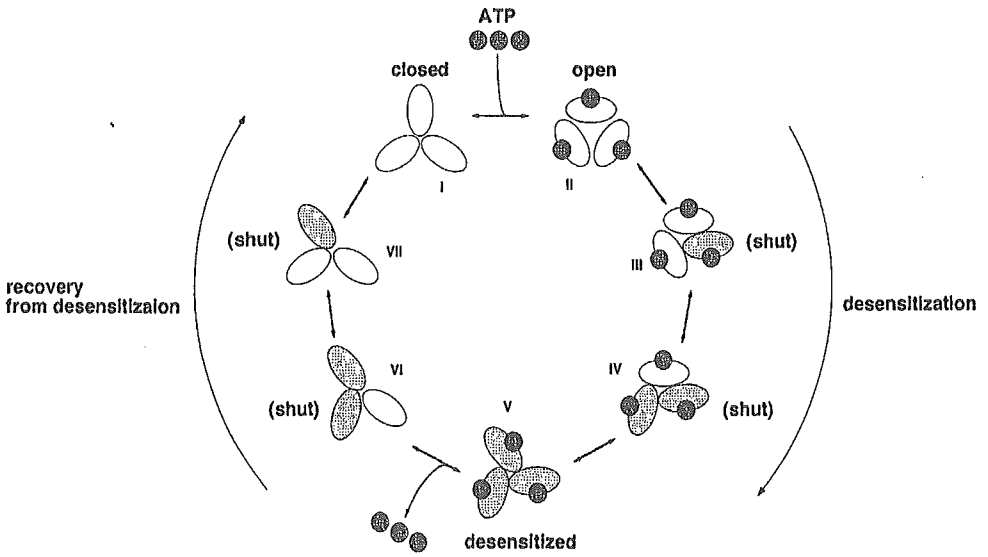

Fig. 6. A schematic model for desensitization and the recovery from desensitization of $P2X_2$ receptor pore mutants. One channel consists of three homogenous subunits. A closed channel (I) is open when ATP molecules bind (II). The open channel is shut when one of the three subunits is shifted to its "desensitized" conformation (III). As for the recovery from desensitization, the desensitized channel (V) is shut until all the subunit is shifted from the "desensitized" conformation (I; closed state).

(Fig. 5). The requirement of multiple exponentials implies that more than one gate should be "on" before the opening of the channel. Based on the trimeric composition of P2X receptors (Nicke et al., 1998; Stoop et al., 1999), these gating mechanisms can schematically explained as shown in Fig. 6. A trimeric $P2X_2$ receptor/channel opens upon the binding of ATP molecules (from state I to state II). The open channel then slowly shifts to the desensitized state. In this process, three subunits independently change their conformations (states III, IV and V), and the channel is shut when one of the subunits has changed its conformation (state III). Thus, the desensitization progresses in the first order kinetics. As for the recovery from the desensitization, the subunits also independently change their conformations (states VI, VII and I), but the channel cannot open until all the subunits have changed the conformations (state I). Thus, the recovery process follows multiple order kinetics.

Although the model shown in Fig. 6 is one of possible explanations, the recovery from the desensitization may, in any case, involves some very slow (in minutes) mechanisms. In rat superior cervical ganglia, $P2X_1$ receptors disappear from cell surface within 1 min after stimulation by agonists, and they are redistributed in the order of minutes at room temperature (Li et al., 2000). Similar redistribution of $P2X_2$ receptors has also been reported in rat hippocampal neurons, and this phenomenon occurs faster (5–10 s) at 32–34 °C (Khakh et al., 2001). The latter appears to require protein kinase C because the phenomenon was not observed when the phosphorylation site was blocked by mutagenesis (T18A). Interestingly, the current permeating through T18A also decays (Khakh et al., 2001) because of its inability to shift to the "second" open state, which appears with the phosphorylated wild type channel during a long exposure to ATP. The relationship of this current decay in T18A and the desensitization of the pore mutants observed in the present study remains to be clarified.

Neither desensitization nor the "inactivation-like" phenomenon was observed with the wild type $P2X_2$ receptor. This implies that the channel pore of the wild type receptor is elaborate enough to escape from these shutting mechanisms. Alternatively, native desensitizing P2X subclasses, such as $P2X_1$ or $P2X_3$, may possess pore structures suitable for desensitization. This view may be favored by the finding that desensitization of chimeric channels constructed from $P2X_1$ and $P2X_2$ are determined by pore forming regions (Werner et al., 1996).

Acknowledgements

We are grateful to H. Sawa for the participation in a part of experiments. This work was partly supported by a Health and Labour Science Research Grant for Research on Advanced Medical Technology from the Ministry of Health, Labour and Welfare, Japan, and a grant-in-aid for scientific research from the Ministry of Education, Science, Sports and Culture, Japan (KAKENHI 13672319) awarded to K.N.

References

Egan, T.M., Haines, W.R., Voigt, M.M., 1998. A domain contributing to the ion channel of ATP-gated $P2X_2$ receptors identified by the substituted cysteine accessibility method. J. Neurosci. 18, 2350–2359.

Ennion, S., Hagan, S., Evans, R.J., 2000. The role of positively charged amino acids in ATP recognition by human $P2X_1$ receptors. J. Biol. Chem. 275, 29361–29367.

Hille, B., 1992a. Classical biophysics of the squid giant axon. Ionic Channels of Excitable Membranes, second edition. Sinauer, Sunderland, MA, pp. 23–58.

Hille, B., 1992b. Ligand-gated channels of fast chemical synapses. Ionic Channels of Excitable Membranes, second edition. Sinauer, Sunderland, MA, pp. 140–169.

Hodgkin, A.L., Huxley, A.F., 1952. The dual effect of membrane potential on sodium conductance in the giant axon of *Loligo*. J. Physiol. 116, 497–506.

Jiang, L.H., Rassendren, F., Surprenant, A., North, R.A., 2000. Identification of amino acid residues contributing to the ATP-binding site of a purinergic P2X receptor. J. Biol. Chem. 275, 34190–34196.

Katz, B., Thesleff, S., 1957. A study of the "desensitization" produced by acetylcholine at the motor end-plate. J. Physiol. 138, 63–80.

Khakh, B.S., 2001. Molecular physiology of P2X receptors and ATP signalling at synapses. Nat. Rev. 2, 165–174.

Khakh, B.S., Smith, W.B., Chiu, C.-S., Ju, D., Davidson, N., Lester, H.A., 2001. Activation-dependent changes in receptor distribution and dendritic morphology in hippocampal neurons expressing $P2X_2$-green fluorescent protein receptors. Proc. Natl. Acad. Sci. U. S. A. 98, 5288–5293.

Li, G.-H., Lee, E.M., Blair, D., Holding, C., Poronnik, P., Cook, D.I., Barden, J.A., Bennett, M.R., 2000. The distribution of P2X receptor clusters on individual neurons in sympathetic ganglia and their redistribution on agonist activation. J. Biol. Chem. 275, 29107–29112.

Nakazawa, K., Ohno, Y., 1996. Dopamine and 5-hydroxytryptamine selectively potentiate neuronal type ATP receptor channels. Eur. J. Pharmacol. 296, 119–122.

Nakazawa, K., Ohno, Y., Inoue, K., 1998. An aspartic acid residue near the second transmembrane segment of ATP receptor/channel regulates agonist sensitivity. Biochem. Biophys. Res. Commun. 244, 599–603.

Nakazawa, K., Sawa, H., Ojima, H., Ishii-Nozawa, R., Takeuchi, K., Ohno, Y., 2002. Size of side-chain at channel pore mouth affects Ca^{2+} block of $P2X_2$ receptor. Eur. J. Pharmacol. 449, 207–211.

North, R.A., 2002. Molecular physiology of P2X receptors. Physiol. Rev. 82, 1013–1067.

Ralevic, V., Burnstock, G., 1998. Receptors for purines and pyrimidines. Pharmacol. Rev. 50, 413–492.

Rassendren, F., Buell, G., Newbolt, A., North, R.A., Surprenant, A., 1997. Identification of amino acid residues contributing to the pore of a P2X receptor. EMBO J. 16, 3446–3454.

Tallarida, R.J., Jacob, L.S., 1979. Kinetics of drug–receptor interaction: interpreting dose–response data. Dose–response relation in Pharmacology. Springer, New York, NY, pp. 49–84.

Werner, P., Seward, E.P., Buell, G.N., North, R.A., 1996. Domains of P2X receptors involved in desensitization. Proc. Natl. Acad. Sci. U. S. A. 93, 15485–15490.

Highlighted paper selected by Editor-in-chief

Modulation of Voltage-Gated Ca^{2+} Current by 4-Hydroxynonenal in Dentate Granule Cells

Tatsuhiro AKAISHI,[a,b] Ken NAKAZAWA,[b] Kaoru SATO,[b] Hiroshi SAITO,[a] Yasuo OHNO,[b] and Yoshihisa ITO*,[a]

[a] *Department of Pharmacology, College of Pharmacy, Nihon University; Funabashi 274–8555, Japan: and* [b] *Division of Pharmacology, National Institute of Health Sciences; Setagaya-ku, Tokyo 158–8501, Japan.*
Received October 11, 2003; accepted December 4, 2003; published online December 12, 2003

Although recent studies have suggested that dentate granule cells play a key role in hippocampal functions, electrophysiological properties in these cells have not been sufficiently explored. In the present study, modification of voltage-gated Ca^{2+} channels by 4-hydroxynonenal (4HN), a major aldehydic product of membrane lipid peroxidation, in cultured dentate granule cells was examined using the whole-cell patch clamp technique. When whole-cell voltage clamp was applied, the cells exhibited a high-voltage-activated Ca^{2+} current, which was totally sensitive to 30 μM Cd^{2+} and partially sensitive to 2 μM nifedipine. 4HN enhanced the Ca^{2+} current in these cells. When L-type Ca^{2+} channels were blocked by application of nifedipine, the enhancement was completely canceled, whereas application of ω-conotoxin-GVIA or ω-agatoxin-IVA, blockers of N- and P/Q-type Ca^{2+} channels, respectively, had no effect. These results suggest that 4HN modulates L-type Ca^{2+} channels in the dentate granule cells, and thereby plays a role in the physiological and pathophysiological responses of these cells to oxidative stress.

Key words dentate granule cell; Ca^{2+} channel; 4-hydroxynonenal; hippocampus

The formation of the hippocampus appears to be essential for certain forms of learning and memory. Several studies have suggested that dentate granule cells play important roles in associative learning.[1—3] Destruction of dentate granule cells with colchicine, or their selective loss following long-term adrenalectomy causes spatial memory deficits and impairments in several learning tasks.[1—3] This memory deficit has been shown to correlate with a loss of dentate granule cells. The dentate gyrus is known to be one of the few regions in the adult mammalian brain that exhibit ongoing neurogenesis. The production of dentate granule cells occurs continuously, even after birth. Their precursors divide in the subgranular proliferative zone at the border of the granule cell layer and the hilus. A proportion of the newborn cells differentiate into neurons, migrate into the granule cell layer, and project to the CA3 region of the hippocampus. Several lines of evidence have suggested that newly generated granule cells play a role in cognition and brain repair.[2,4,5] Furthermore, it has already been reported that cultured dentate granule cells provide a faithful and useful model of mossy fiber sprouting.[6]

Although dentate granule cells play important roles in hippocampal functions, the electrophysiological properties of these cells have not been clarified sufficiently. Both *in situ* hybridization and immunocytochemical experiments have demonstrated that the level of L-type Ca^{2+} channel subunit expression is higher in the dentate granule cell layer than in any other area of the hippocampus.[7] Thus, it is very important to characterize in detail the Ca^{2+} currents that arise through voltage-gated Ca^{2+} channels (VGCCs) in dentate granule cells if we are to understand their physiological and pathological relevance.

Oxidative stress is implicated in a variety of physiological and pathophysiological processes such as immune defense, ischemia, and neurodegenerative diseases (*e.g.*, Alzheimer's disease, AD).[8—11] Oxidative stress arising from excessive production or decreased clearance of reactive oxygen species (ROS) can result in the accumulation of ROS, cellular damage, and eventual cell death. Indeed, the molecular and cellular events underlying the neuronal death induced by oxidative stress have been clarified in the HT-22 hippocampal cell line and in cortical neurons.[12—14]

Levels of lipid peroxidation are increased in the brain of AD patients, and the levels of thiobarbituric-acid-reactive substances are elevated in most regions of the AD brain compared with controls.[15] One of the lipid peroxidation products, 4-hydroxynonenal (4HN), has been shown to play important roles in the neuronal cell death associated with many different neurodegenerative diseases, such as AD,[8,9] Parkinson's disease,[16] and sporadic amyotrophic lateral sclerosis.[17] Several studies have shown that 4HN is generated in response to oxidative insults and can induce neuronal apoptosis.[18—20] Furthermore, it has been demonstrated that the mechanisms underlying the neuronal damage induced by 4HN involves the disturbance of ion homeostasis.[9] Despite the importance of 4HN-induced neuronal damage, the modulation of Ca^{2+}-channel activity by 4HN has not been adequately studied in dentate granule cells.

In order to clarify this issue, we employed a dissociated cell culture system of dentate granule cells, the whole-cell patch clamp technique, characterized the properties of the Ca^{2+} current in dentate granule cells, and investigated whether and how 4HN could affect the current in these cells.

MATERIALS AND METHODS

All experiments in this study were performed in accordance with the guidelines of the National Institute of Health Sciences.

Cell Culture Unless otherwise specified, neurons were cultivated in Neurobasal medium (Life Technologies, Gaithersburg, MD, U.S.A.) supplemented with 73 μg/ml L-

* To whom correspondence should be addressed. e-mail: yoshiito@pha.nihon-u.ac.jp

glutamine (Wako, Osaka, Japan) and 2% B-27 supplement (Life Technologies). Three- to 4-d-old Wistar rat pups (Nihon SLC, Shizuoka, Japan) were deeply anesthetized with ether, and the hippocampi were removed. The dentate gyrus was dissociated from the hippocampus with extreme care and under visual control. The dentate gyrus was cut into pieces, which were then treated with 0.25% trypsin (Difco, Detroit, MI, U.S.A.) and 0.01% deoxyribonuclease I (Sigma, St Louis, MO, U.S.A.) at 37 °C for 30 min. The incubation was terminated by addition of heat-inactivated horse serum (HS; Cell Culture, Cleveland, OH, U.S.A.). The tissue fragments were centrifuged at 1200 rpm for 5 min. The supernatant was removed and the pellet was suspended in a mixture of 50% Neurobasal medium/B-27 supplement and 50% astrocyte-conditioned medium (ACM), which was prepared according to Ikegaya *et al.*[6] In general, cultured astrocytes are known to posses a range of neurotrophic activities in culture and have been found to express mRNA for neurotrophic factors such as ciliary neurotrophic factor, nerve growth factor, and neurotrophin 3.[21] The suspension was gently triturated until visibly dispersed, and then filtered through a nylon net. The cells were plated at a density of 2.0×10^4 cells/cm^2 onto round, 13-mm-diameter glass cover slips (Matsunami, Osaka, Japan) that had been coated with polyethyleneimine (Sigma). In order to support the adhesion and survival of neurons, we used the culture medium containing ACM for 24 h after the plating. The culture medium was changed to ACM-free Neurobasal/B-27 medium thereafter. The cultures were maintained in the same medium at 37 °C in a humidified incubator with 5% CO_2–95% air. The medium was replaced twice a week. Experiments were performed with cultures that had been maintained for 7 d.

Immunocytochemistry Twenty-four hours before the preparation of cell cultures, the rat pups were injected intraperitoneally with 5-bromo-2′-deoxyuridine (BrdU, 100 mg/kg body weight, in saline; Wako). Seven days after the dissociation, cells were fixed with 4% paraformaldehyde in 0.1 M phosphate buffer (pH 7.4) for 30 min at 4 °C. For DNA denaturation, cells were incubated in 2 M HCl for 30 min at room temperature, rinsed twice with PBS, and incubated in 0.1 M Tris–HCl (pH 7.5) for 5 min. After two washes with PBS, cells were incubated for 1 h in PBS containing 2% normal HS and then incubated overnight at 4 °C in primary antibody (mouse anti-BrdU; Roche, Mannheim, Germany) diluted in the HS-containing PBS. After washing three times with PBS, cells were incubated in secondary antibody (biotinylated horse anti-mouse; Vector Laboratories, Burlingame, CA, U.S.A.) diluted in the HS-containing PBS for 1.5 h and then rinsed three times with PBS. Endogenous peroxidase activity was blocked by incubating the cells in 0.3% H_2O_2 dissolved in methanol for 1 h. After washing three times with PBS, cells were incubated in avidin–biotin–peroxidase complex (ABC Elite kit; Vector Laboratories) for 1 h and then rinsed a further three times with PBS. The BrdU labeling was visualized using 3,3′-diaminobenzidine tetrahydrochloride (DAB; Wako). Cells were preincubated for 5 min in DAB dissolved in PBS (0.2 mg/ml) without H_2O_2, followed by addition of H_2O_2 solution (final concentration, 0.01%). The peroxidase reaction was allowed to proceed for about 5—10 min. Cells were washed repeatedly in PBS, and then rinsed with water. To count BrdU-labeled cells, at least three areas (each $211\times317\ \mu m^2$) were selected randomly for each sample.

Electrophysiology Whole-cell recordings were made with the aid of glass patch pipettes (2—5 MΩ) filled with 100 mM CsCl, 2 mM $MgCl_2$, 10 mM EGTA, 10 mM *N*-(2-hydroxyethyl) piperazine-*N*′-ethanesulfonic acid (Hepes), 15 mM tetraethylammonium chloride, 5 mM Mg-ATP, 20 mM creatine phosphate, and 50 U/ml creatine kinase (the pH was adjusted to 7.3 with CsOH). The external solution contained the following: 130 mM NaCl, 5 mM $CaCl_2$, 2 mM $MgCl_2$, 10 mM Hepes, 10 mM glucose, 5 mM 4-aminopyridine and 500 nM tetrodotoxin (the pH was adjusted to 7.4 with NaOH). Membrane currents were recorded under voltage-clamp conditions using a patch-clamp amplifier (Nihon Kohden, Tokyo, Japan) and data acquisition/analysis software (pCLAMP; Axon Instruments CA, U.S.A.), with filtering at 1 kHz. All of the experiments were performed at room temperature.

Drugs and Their Application The pharmacological properties of the Ca^{2+} current in dentate granule cells were studied by adding the appropriate drugs to the external solution. Nifedipine (Sigma) was prepared as a 500× stock solution in ethanol. Ni^{2+} and Cd^{2+} were freshly prepared daily. In some recordings, Ba^{2+} was used as a charge carrier instead of Ca^{2+}. 4HN (Cayman Chemical, Ann arbor, MI, U.S.A.) was prepared as a 1000× stock solution in ethanol. ω-Conotoxin-GVIA and ω-agatoxin-IVA were purchased from Peptides Institute (Osaka, Japan) and prepared as 100 μM stock solutions in saline. The effects of 4HN on the Ca^{2+} current were studied using 4HN added to Locke's buffer (154 mM NaCl, 5.6 mM KCl, 2.3 mM $CaCl_2$, 1.0 mM $MgCl_2$, 3.6 mM $NaHCO_3$, 10 mM glucose, and 5 mM Hepes, pH 7.2), according to the method described by Mark *et al.*[9] Immediately before experimental treatment, the culture medium was replaced with Locke's buffer. In all experiments, an equivalent volume of vehicle was added to control cultures.

RESULTS

Identification of Dentate Granule Cells The vast majority of neurons in the dentate gyrus of the hippocampus are granule cells,[22] but contamination by a small number of pyramidal cells or interneurons is still possible. To exclude this possibility, we carefully identified dentate granule cells in a prepared cell population based on their size and morphology. Phase-contrast photographs of dentate gyrus cell cultures are shown in Fig. 1A. In these cultures, we observed quite a large number of dentate granule cells, which have small and round or oval cell bodies (Fig. 1A, middle). These cells possessed one or two thin processes. In the same cultures, a subpopulation of neurons different from dentate granule cells was identified. This subpopulation included neurons displaying a pyramidal-cell-like shape (Fig. 1A, right) or a nongranule-cell-, nonpyramidal-cell-like shape (data not shown). To compare granule cells with the remaining neurons, the width and the length of their cell bodies were measured, and the results are summarized as histograms (Fig. 1B.) In our cell cultures, neither the width nor the length of the cell bodies of the total cell population exhibited a Gaussian distribution (Fig. 1B, top). However, the population of dentate granule cells, selected by the visual criteria stated above, exhibited a Gaussian distribution (Fig. 1B, mid-

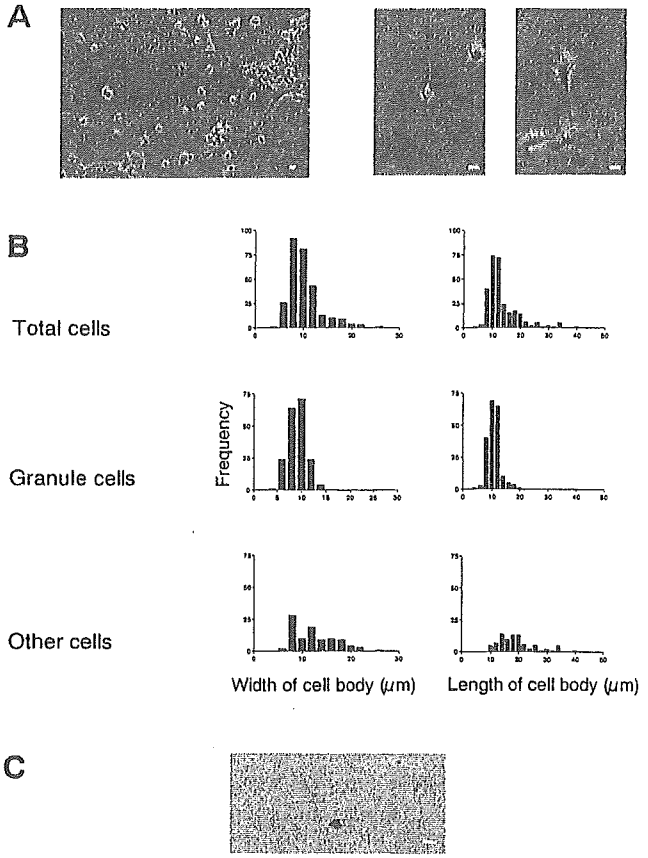

Fig. 1. Neurons in Dentate Gyrus Cultures

A. Phase-contrast photographs of 7-d-cultured dentate gurus cells. Representative photomicrographs showing cultured dentate gyrus neurons (left), a granule cell (middle), and pyramidal cells (right). B. Histograms showing the size distributions of dentate gyrus neurons (the total population of neurons in dentate gyrus cultures is shown at the top, the granule cells are shown in the middle, and the remaining neurons are shown at the bottom). The width (left) and the length of the cell bodies (right) are shown for each cell population. C. Immunochemical identification of newborn dentate granule cells. BrdU-labeled cells are evident in the photomicrograph of dentate gyrus cultures. No BrdU-positive label was observed in neurons other than the granule cells in these cultures (data not shown). The scale bar=10 μm.

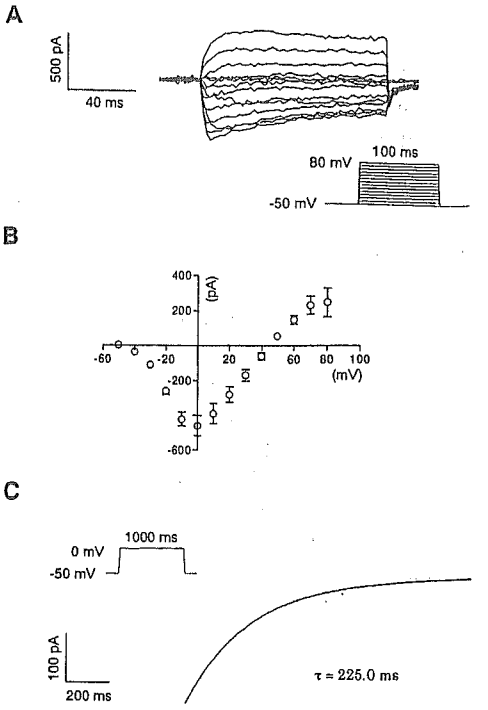

Fig. 2. Ca^{2+} Current in 7-d-Cultured Cells

Outward currents were blocked by Cs^+, tetraethylammonium and 4-aminopyridine. Recordings were made with 500 nM tetrodotoxin to block voltage-gated Na^+ channels. A. Depolarizing command pulses from a holding potential of −50 mV elicited the Ca^{2+} current. B. Averaged current–voltage (*I–V*) relationship of the Ca^{2+} current (n=26). The threshold of activation was at about −30 mV, and the current peaked at 0 mV. Each symbol and bar represent the mean and S.E.M., respectively. C. An example of a single exponential fit to the current decay. The fit was superimposed on an original current trace that was obtained by a command potential to 0 mV.

dle). For these granule cells, the averaged cell body width and length were 8.6±0.1 μm and 10.4±0.2 μm, respectively (mean±S.E.M., n=198). The width and the length of the cell bodies of the remaining "non-granule cells" were 13.5±0.5 μm and 19.4±0.7 μm, respectively (n=110).

Although most mammalian neurons are formed before birth, the production of dentate granule cells continues until adulthood. To examine whether the dentate granule cells identified by our criteria exhibited neurogenesis, we quantified newly generated neurons using BrdU immunochemistry method. As shown in Fig. 1C, we observed BrdU-labeled dentate granule cells, indicating that newly generated dentate granule cells existed in the cultures. From the quantitative analysis, 14.1±2.7% (mean±S.E.M.) of total dentate granule cells were BrdU positive. These results suggest that the dentate granule cells in our cell cultures possessed characteristics similar to those identified *in vivo* with respect to their shape, size, and capacity for neurogenesis, and that dentate granule cells can therefore be distinguished using our criteria.

Whole-cell Ca^{2+} Currents in Dentate Granule Cells Electrophysiological experiments were performed on the cultured dentate granule cells. In many peripheral and central neurons, Ca^{2+} currents can be grouped according to their activation thresholds into low-voltage-activated (LVA) or high-voltage-activated (HVA) Ca^{2+} currents. The LVA currents are activated at between −70 and −40 mV and inactivate rapidly. The HVA currents are activated at around −30 mV and inactivate slowly.[23] Ca^{2+} currents elicited in cultured dentate granule cells by depolarizing voltage steps between −50 and 80 mV are shown in Fig. 2A. The voltage steps were applied for 100 ms from a holding potential of −50 mV. Ca^{2+} currents were activated at −30 mV and more positive potentials, and the maximal current was observed at 0 mV (−459.3±58.1 pA; mean±S.E.M. n=26; Fig. 2B). The current activated by a 1-s depolarizing voltage step exhibited a clear decay, and this decay was analyzed by fitting monoexponential functions (Fig. 2C). The time constant for the decay at 0 mV was 223.0±27.3 ms (n=10).

The HVA currents are characterized by a much higher permeability for Ba^{2+} than for Ca^{2+}.[24] Substitution of Ca^{2+} by an equimolar concentration of Ba^{2+} increases the amplitude of the HVA currents. In the cultured dentate granule cells, the current amplitude was increased by 56.0±13.1% (n=6) at a test pulse of 0 mV when 5 mM Ca^{2+} was replaced by 5 mM Ba^{2+} (Fig. 3A). Inorganic ions such as Ni^{2+} or Cd^{2+} are potent blockers of various types of Ca^{2+} currents. While such divalent ions cause a relatively nonspecific block at concentrations in the millimolar range,[25,26] they show some specificity when used in the micromolar concentration range. In most neurons, 30 μM Cd^{2+} blocks selectively the HVA currents, while the LVA currents remain almost unaffected. In

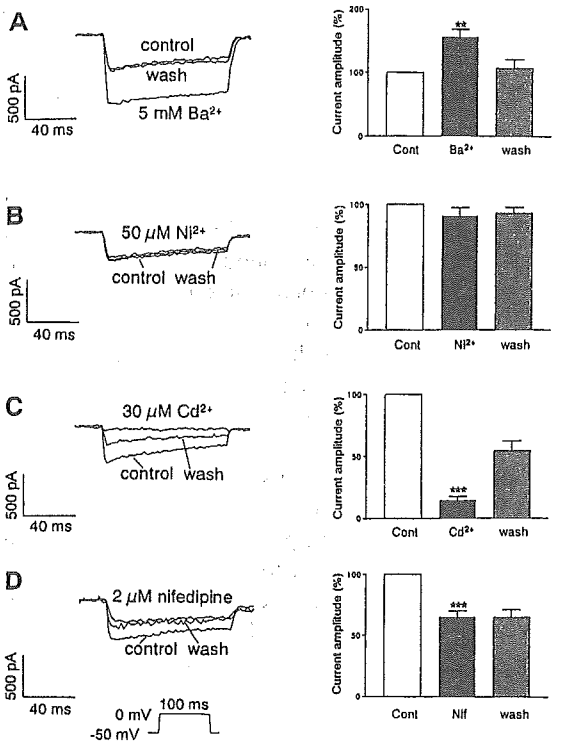

Fig. 3. Effects of Replacement of Ca^{2+} by Ba^{2+} (A) and Application of Ca^{2+} Channel Blockers (B—D) on the Ca^{2+} Current

The Ca^{2+} current was elicited by a voltage step to 0 mV. Representative current traces of Ca^{2+} current (left) and a summary of the averaged data (right) are shown. Also shown are the effects of replacement of 5 mM Ca^{2+} by 5 mM Ba^{2+} (A), 50 μM Ni^{2+} (B), 30 μM Cd^{2+} (C), and 2 μM nifedipine (D). Values are the mean±S.E.M. of data from 5—8 neurons from at least three separate cultures (**$p<0.01$, ***$p<0.001$, paired t-test).

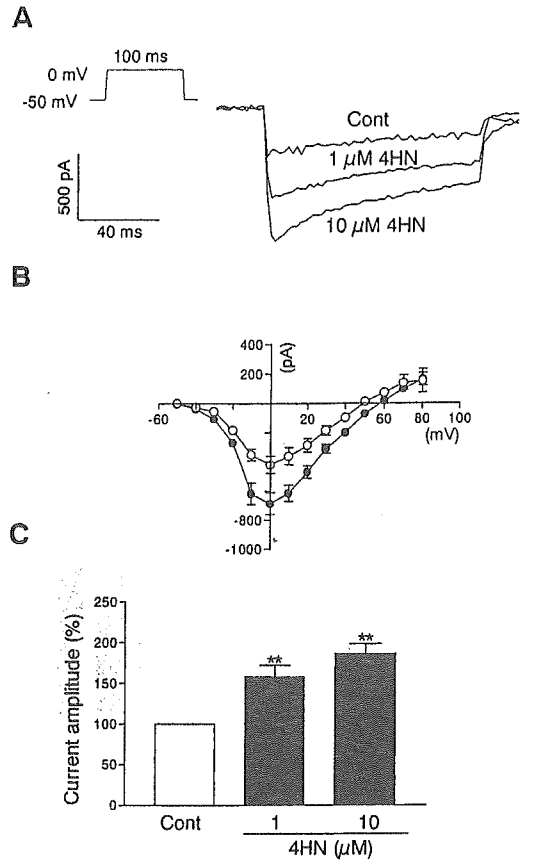

Fig. 4. 4-Hydroxynonenal (4HN) Enhances the Ca^{2+} Current in Dentate Granule Cells

A. Representative recordings of the Ca^{2+} current in cells that had been treated for 2 h with either 1 or 10 μM 4HN. Control cells had been treated with 0.02% ethanol (vehicle). B. Averaged I–V relationship in cells that had been exposed for 2 h to either the vehicle (○, $n=10$) or 10 μM 4HN (●, $n=9$). C. Summarized data of the peak Ca^{2+} current in cells exposed for 2 h to the indicated concentrations of 4HN. Values are the mean±S.E.M. from 10—21 neurons from at least five separate cultures (**$p<0.01$, ANOVA followed by Dunnett's multiple range test).

contrast, 50 μM Ni^{2+} preferentially reduces the LVA currents. Figure 3B shows the effect of 50 μM Ni^{2+} on the Ca^{2+} current elicited by a test pulse to 0 mV. The Ca^{2+} current was reduced by 9.4±6.9% on average ($n=6$). With 30 μM Cd^{2+}, the Ca^{2+} current was decreased by 87.8±3.4% ($n=5$; Fig. 3C). Nifedipine, a dihydropyridine HVA Ca^{2+}-current blocker, depressed the Ca^{2+} current by 33.8±6.2% ($n=8$; Fig. 3D).

Effects of 4HN on Ca^{2+} Currents in the Dentate Granule Cells Pretreatment of dentate granule cells with 1 μM 4HN for 2 h resulted in a significant increase (58.1±14.4%) in the amplitude of the Ca^{2+} current. The current amplitude was increased by 28% in neurons exposed to 10 μM 4HN (Fig. 4). The current–voltage relationships in the absence or presence of 4HN showed that the voltage dependence remained unchanged in neurons exposed to 4HN (Fig. 4B). Cultured hippocampal neurons express VGCCs of the L, N, and P/Q types, and the majority of the whole-cell Ca^{2+} current is attributed to L-type Ca^{2+} channels.[27,28] To determine which types of VGCCs were affected by 4HN, we employed pharmacological agents that block specific channel types. In control cultures, addition of 3 μM ω-conotoxin-GVIA, a blocker of N-type Ca^{2+} channels, 2 μM nifedipine, a blocker of L-type Ca^{2+} channels, and 0.3 μM ω-agatoxin-IVA , a blocker of P/Q-type Ca^{2+} channels, resulted in 20.7, 34.8, and 23.0% decreases in the amplitude of the Ca^{2+} current, respectively (Fig. 5B). In 4HN-treated neurons, ω-conotoxin-GVIA caused a 16.4% decrease, nifedipine caused a 90.0% decrease, and ω-agatoxin-IVA caused a 22.8% decrease in the amplitude of the Ca^{2+} current (Fig. 5B). These results suggest that the increase is due mainly to an increase in a current that is mediated through L-type Ca^{2+} channels.

DISCUSSION

In the present study, a dissociated culture system rich in dentate granule cells obtained from postnatal rats was employed to characterize their electrophysiological properties. Although effective electrophysiological studies using adult hippocampal slices have been reported recently, we employed a cell culture system using dissected dentate gyrus and identified dentate granule cells, which we have used previously to examine the effects of 4HN on cell death in various neuronal preparations such as cultured hippocampal neurons,[20] PC12,[19] and cultured cerebellar granule neurons;[18] we have also used this protocol for a preliminarily study of cultured Ammon's horn neurons and dentate gyrus neurons (our unpublished data). Similar culture approaches using dentate gyrus cell have already been reported,[29,30] and the dentate granule cell culture system has been already shown to be a faithful and useful model of mossy fiber sprouting.[6] However, there have not been sufficient analyses of cell properties to allow the identification of dentate granule cells in these studies. In the present study, we carefully identified dentate

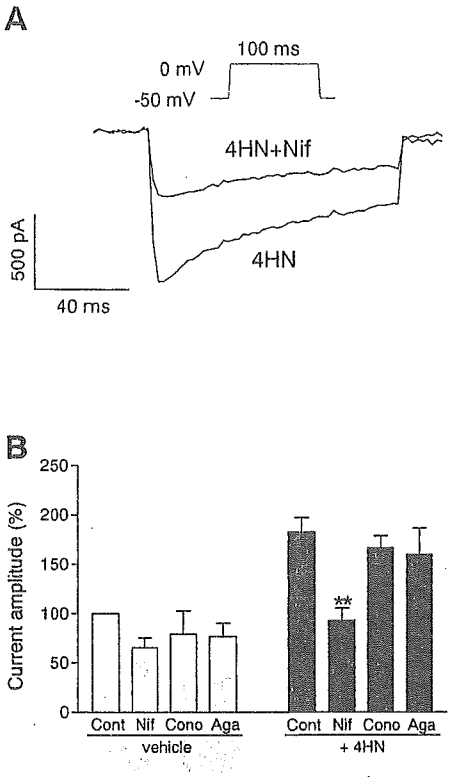

Fig. 5. Effects of Ca^{2+} Channel Blockers on the Ca^{2+} Current in Dentate Granule Cells

A. Representative current traces of the Ca^{2+} current. B. Summarized data of current amplitudes obtained in the absence (Cont) or presence of the blockers for specific subtypes of VGCCs (nifedipine, Nif; ω-conotoxin-GVIA, Cono; ω-agatoxin-IVA, Aga) from control cultures (vehicle; open columns) and cultures treated for 2 h with 10 μM 4HN (+4HN). Values are the mean±S.E.M. from 6—14 neurons. ** $p<0.01$ compared with corresponding control values determined by ANOVA followed by Dunnett's multiple range test.

granule cells, and then used these cells for the subsequent investigations. The cells used for the electrophysiological investigations were small in size and round or oval in shape. Their morphological characteristics are consistent with those that have been reported for dentate granule cells.[29] Moreover, the cells were stained with BrdU, a marker of dividing cells, indicating that they possessed the capacity for neurogenesis after birth. These results suggest that the identified cells were indeed dentate granule cells. Therefore, the dentate granule cells identified by our criteria were chosen for experiments including electrophysiological analyses.

High levels of subunit expression of L-type Ca^{2+} channels have been found in the dentate granule cell layer.[7] In the present study, we investigated the basic properties of the Ca^{2+} current using dentate granule cells. The threshold of activation of the Ca^{2+} current in these cells was about −30 mV. The Ca^{2+} current became maximal at 0 mV. Their kinetics compare well with those of the HVA Ca^{2+} currents reported in various other neuronal preparations.[31] With a depolarizing step of 1 s duration, the current decay could be fitted by monoexponential functions. By using the inorganic Ca^{2+} antagonists Cd^{2+}, a HVA Ca^{2+}-current blocker, and Ni^{2+}, a T-type Ca^{2+}-channel blocker, as pharmacological tools, the Ca^{2+} currents in dentate granule cells were characterized further. The Ca^{2+} current in these cells was highly sensitive to a low concentration (30 μM) of Cd^{2+}, as has been reported previously for HVA Ca^{2+} currents.[24,32,33] Unlike the LVA Ca^{2+} currents described previously,[25,26] the Ca^{2+} current in the granule cells was not particularly sensitive to a micromolar concentration (50 μM) of Ni^{2+}. Moreover, nifedipine, a dihydropyridine Ca^{2+}-channel antagonist, blocked a large proportion of the current. These findings are consistent with a high expression of the L-type Ca^{2+} channel shown by *in situ* hybridization and by immunocytochemical studies.[7,34] In the present study, two types of dentate granule cells [*i.e.* BrdU positive (newly generated type) and BrdU negative (relatively mature type) cells] have been found. Although technical limitations prevented us from being able to distinguish between them in electrophysiological experiments, we did not observe any significant differences throughout the electrophysiological experiments. Further detailed investigations using different experimental techniques will be necessary to clarify this problem.

Oxidative injury to neurons in regions responsible for learning and memory processes, such as the hippocampus, is believed to play a role in the pathogenesis of AD.[8,10] Furthermore, 4HN has been shown to play important roles in the neuronal cell death induced by oxidative insults. Although recent reports have demonstrated that oxidative stress modulates the activity of several types of channels in cultured hippocampal neurons and adult rat hippocampal slices,[35,36] the effects of 4HN on the Ca^{2+} current in dentate granule cells are unclear. In the present study, the amplitude of the Ca^{2+} current in 4HN-treated dentate granule cells was significantly larger than in the untreated cells. When L-type Ca^{2+} channels were blocked by nifedipine, the current augmentation by 4HN was canceled, whereas the blocking of N- or P/Q-type channels by ω-conotoxin-GVIA or ω-agatoxin-IVA, respectively, had no effect. It has been reported that the blocking of L-type Ca^{2+} channels attenuates amyloid β protein (Aβ)-induced cell death,[37,38] whereas the blocking of N- or P/Q-type Ca^{2+} channels have little effect.[39] In addition, this Aβ-induced influx of Ca^{2+} is mediated by free radicals. These findings also suggest that oxidative stress increases the Ca^{2+} influx mediated through L-type Ca^{2+} channels.

In the present study, 1—10 μM 4HN significantly enhanced the Ca^{2+} current. These concentrations of 4HN are compatible with those that have been measured in hippocampal neurons after exposure to Aβ.[9] The exact mechanisms whereby 4HN selectively enhances the nifedipine-sensitive Ca^{2+} current in cultured dentate granule cells remain to be elucidated. Currents that originate through VGCCs are known to be increased by the phosphorylation of channel α subunit proteins. Tyrphostins, a family of protein tyrosine kinase inhibitors, protect the nerve cell line HT-22, as well as rat primary neurons, from the cell death induced by oxidative toxicity.[14] In addition, the levels of phosphorylation of the NMDA receptor subunit NR1 are increased in neurons exposed to 4HN.[40] 4HN may directly or indirectly increase phosphorylation of the α subunit of L-type Ca^{2+} channels. L-type Ca^{2+} channels are abundant in dentate granule cells, and so the augmentation of these channels by 4HN may be implicated in pathophysiological processes.

Acknowledgements This work was partly supported by Health and Labour Science Research Grants for Research on Advanced Medical Technology from the Ministry of Health, Labour and Welfare, Japan and a Grant-in-aid for Scientific Research from The Ministry of Education, Culture, Sports,

Science, and Technology, Japan (KAKENHI 13672319) awarded to K.N.

REFERENCES

1) Conrad C. D., Roy E. J., *J. Neurosci.*, **13**, 2582—2590 (1993).
2) Lemaire V., Koehl M., Le Moal M., Abrous D. N., *Proc. Natl. Acad. Sci. U.S.A.*, **97**, 11032—11037 (2000).
3) McNaughton B. L., Barnes C. A., Meltzer J., Sutherland R. J., *Exp. Brain Res.*, **76**, 485—496 (1989).
4) Liu J., Solway K., Messing R. O., Sharp F. R., *J. Neurosci.*, **18**, 7768—7778 (1998).
5) van Praag H., Schinder A. F., Christie B. R., Toni N., Palmer T. D., Gage F. H., *Nature* (London), **415**, 1030—1034 (2002).
6) Ikegaya Y., Nishiyama N., Matsuki N., *Neuroscience*, **98**, 647—659 (2000).
7) Chin H., Smith M. A., Kim H. L., Kim H., *FEBS Lett.*, **299**, 69—74 (1992).
8) Mark R. J., Blanc E. M., Mattson M. P., *Mol. Neurobiol.*, **12**, 211—224 (1996).
9) Mark R. J., Lovell M. A., Markesbery W. R., Uchida K., Mattson M. P., *J. Neurochem.*, **68**, 255—264 (1997).
10) Yankner B. A., *Neuron*, **16**, 921—932 (1996).
11) Urabe T., Yamasaki Y., Hattori N., Yoshikawa M., Uchida K., Mizuno Y., *Neuroscience*, **100**, 241—250 (2000).
12) Ishige K., Schubert D., Sagara Y., *Free Radic. Biol. Med.*, **30**, 433—446 (2001).
13) Ishige K., Chen Q., Sagara Y., Schubert D., *J. Neurosci.*, **21**, 6069—6076 (2001).
14) Sagara Y., Ishige K., Tsai C., Maher P., *J. Biol. Chem.*, **277**, 36204—36215 (2002).
15) Miranda S., Opazo C., Larrondo L. F., Muñoz F. J., Ruiz F., Leighton F., Inestrosa N. C., *Prog. Neurobiol.*, **62**, 633—648 (2000).
16) Yoritaka A., Hattori N., Uchida K., Tanaka M., Stadtman E. R., Mizuno Y., *Proc. Natl. Acad. Sci. U.S.A.*, **93**, 2696—2701 (1996).
17) Pedersen W. A., Fu W., Keller J. N., Markesbery W. R., Appel S., Smith R. G., Kasarskis E., Mattson M. P., *Ann. Neurol.*, **44**, 819—824 (1998).
18) Ito Y., Arakawa M., Ishige K., Fukuda H., *Neurosci. Res.*, **35**, 321—327 (1999).
19) Ito Y., Kosuge Y., Sakikubo T., Horie K., Ishikawa N., Obokata N., Yokoyama E., Yamashina K., Yamamoto M., Saito H., Arakawa M., Ishige K., *Neurosci. Res.*, **46**, 119—125 (2003).
20) Kosuge Y., Koen Y., Ishige K., Minami K., Urasawa H., Saito H., Ito Y., *Neuroscience*, **122**, 885—895 (2003).
21) Rudge J. S., Alderson R. F., Pasnikowski E., McClain J., Ip N.Y., Lindsay R. M., *Eur. J. Neurosci.*, **4**, 459—471 (1992).
22) Seress L., Pokorny J., *J. Anat.*, **133**, 181—195 (1981).
23) Carbone E., Lux H. D., *Nature* (London), **310**, 501—502 (1984).
24) Fox A. P., Nowycky M. C., Tsien R. W., *J. Physiol.*, **394**, 149—172 (1987).
25) Muller T. H., Misgeld U., Swandulla D., *J. Physiol.*, **450**, 341—362 (1992).
26) Ozawa S., Tsuzuki K., Iino M., Ogura A., Kudo Y., *Brain Res.*, **495**, 329—336 (1989).
27) Blalock E. M., Porter N. M., Landfield P. W., *J. Neurosci.*, **19**, 8674—8684 (1999).
28) Furukawa K., Mattson M. P., *J. Neurochem.*, **70**, 1876—1886 (1998).
29) Baranes D., Lopez-Garcia J. C., Chen M., Bailey C. H., Kandel E. R. *Proc. Natl. Acad. Sci. U.S.A.*, **93**, 4706—4711 (1996).
30) Boss B. D., Gozes I., Cowan W. M., *Brain Res.*, **433**, 199—218 (1987).
31) Bean B. P., *Annu. Rev. Physiol.*, **51**, 367—384 (1989).
32) Mogul D. J., Fox A. P., *J. Physiol.*, **433**, 259—281 (1991).
33) Toselli M., Taglietti V., *Neurosci. Lett.*, **112**, 70—75 (1990).
34) Ahlijanian M. K., Westenbroek R. E., Catterall W. A., *Neuron*, **4**, 819—832 (1990).
35) Muller W., Bittner K., *J. Neurophysiol.*, **87**, 2990—2995 (2002).
36) Sah R., Galeffi F., Ahrens R., Jordan G., Schwartz-Bloom R. D., *J. Neurochem.*, **80**, 383—391 (2002).
37) Weiss J. H., Pike C. J., Cotman C. W., *J. Neurochem.*, **62**, 372—375 (1994).
38) Abe K., Kimura H., *J. Neurochem.*, **67**, 2074—2078 (1996).
39) Ueda K., Shinohara S., Yagami T., Asakura K., Kawasaki K., *J. Neurochem.*, **68**, 265—271 (1997).
40) Lu C., Chan S. L., Haughey N., Lee W. T., Mattson M. P., *J. Neurochem.*, **78**, 577—589 (2001).

ELSEVIER

Neuroscience Letters 356 (2004) 25–28

Neuroscience Letters

www.elsevier.com/locate/neulet

Hydrogen peroxide modulates whole cell Ca^{2+} currents through L-type channels in cultured rat dentate granule cells

Tatsuhiro Akaishi[a,b], Ken Nakazawa[b], Kaoru Sato[b], Hiroshi Saito[a], Yasuo Ohno[b], Yoshihisa Ito[a,*]

[a]*Department of Pharmacology, College of Pharmacy, Nihon University, 7-7-1 Narashinodai, Funabashi-shi, Chiba 274-8555, Japan*
[b]*Division of Pharmacology, National Institute of Health Sciences, Setagaya, Tokyo 158-8501, Japan*

Received 23 October 2003; received in revised form 12 November 2003; accepted 13 November 2003

Abstract

Modification of voltage-gated Ca^{2+} channels by hydrogen peroxide, a membrane-permeable form of reactive oxygen species, in cultured dentate granule cells was examined using the whole cell patch clamp technique. Pretreatment with hydrogen peroxide (1 and 10 μM) for 2 h enhanced the Ca^{2+} current without affecting its voltage dependence. The enhancement was completely cancelled by 1 mM glutathione, an antioxidant, and 2 μM nifedipine, an L-type Ca^{2+} channel blocker. In contrast, the enhancement of the Ca^{2+} current was not mimicked by pretreatment with 10 μg/ml tunicamycin, an endoplasmic reticulum stressor. These results suggest that oxidative stress induced by hydrogen peroxide selectively regulates the activity of L-type Ca^{2+} channels.

Keywords: Hydrogen peroxide; Oxidative stress; Patch clamp; Ca^{2+} channel; Hippocampus; Dentate granule cell

Oxidative stress is implicated in many different neurodegenerative diseases, such as Alzheimer's disease (AD) [16], Parkinson's disease [17], and sporadic amyotrophic lateral sclerosis [13]. Oxidative stress arising from excessive production or decreased clearance of reactive oxygen species (ROS) can result in accumulation of ROS, cellular damage, and eventual cell death. Indeed, molecular and cellular events underlying neuronal death induced by oxidative stress have been demonstrated in the hippocampal cell line HT-22 and in cortical neurons [3,4,14]. Endogenous glutamate depletes intracellular glutathione (GSH), leading to the accumulation of ROS and an increase in Ca^{2+} influx, which finally causes neuronal death. It has been reported that apomorphine, a dopamine D_4 agonist, inhibits oxidative stress-induced neuronal cell death in HT-22 cells and primary rat cortical neurons [3], and the protective effects of apomorphine on cell death are mediated, at least in part, by regulation of the cGMP-operated Ca^{2+} channel. This report also suggests that ROS-induced Ca^{2+} influx plays important roles in oxidative stress-mediated neuronal damage. Several pathways can lead to such Ca^{2+} elevation in neurons, and a major pathway for Ca^{2+} influx across the plasma membrane is voltage-gated Ca^{2+} channels (VGCCs). VGCCs are involved in various neuronal functions, including neurotransmitter release, synaptic plasticity, and gene expression [11]. Excessive Ca^{2+} influx through these channels contributes to neuronal death in pathological settings such as AD [5,11]. Recent studies have demonstrated that hydrogen peroxide (H_2O_2), a membrane-permeable form of ROS, modulates the activities of several types of ion channels [12,15] and these changes in channel activities may also be related to pathological events. Despite the importance of VGCCs, modulation of Ca^{2+} channel activity by oxidative stress has not been adequately studied. To clarify whether ROS alter Ca^{2+} channel activity, we used the whole cell patch clamp technique to examine the effects of H_2O_2 on VGCCs in cultured dentate granule cells from postnatal rats.

All experiments in this study were performed in accordance with the guidelines of the National Institute of Health Sciences. For the preparation of cultured dentate granule cells, we employed with modification a cell culture system described by Ikegaya et al. [2]. Briefly, 3- to 4-day-old Wistar rat pups (Nihon SLC, Shizuoka, Japan) were deeply anesthetized with ether, and the hippocampi were removed. The dentate gyrus was dissected out and incubated with 0.25% trypsin (Difco, Detroit, MI) and 0.01%

* Corresponding author. Tel./fax: +81-474-65-5832.
E-mail address: yoshiito@pha.nihon-u.ac.jp (Y. Ito).

0304-3940/03/$ - see front matter © 2003 Elsevier Ireland Ltd. All rights reserved.
doi:10.1016/j.neulet.2003.11.012

deoxyribonuclease I (Sigma, St Louis, MO) at 37 °C for 30 min. The pellet was suspended in a mixture of 50% Neurobasal medium (Life Technologies, Gaithersburg, MD) containing 2% B-27 supplement (Life Technologies) and 73 μg/ml L-glutamine (Wako, Osaka, Japan), and 50% astrocyte-conditioned medium. The suspension was gently triturated, and passed through two sheets of nylon net. The cells were plated at a density of 2.0×10^4 cells/cm^2 onto 13 mm round glass coverslips (Matsunami, Osaka, Japan) coated with polyethyleneimine. One day after the plating, the ACM-containing medium was changed to ACM-free Neurobasal medium containing 2% B-27 supplement and 73 μg/ml L-glutamine. The medium was changed twice a week thereafter. The cells were cultured at 37 °C in a humidified 5% CO_2/95% air atmosphere.

Electrophysiological experiments were performed with cells that had been cultured for 7–9 days. Immediately before experimental treatment, the culture medium was replaced with Locke's solution (154 mM NaCl, 5.6 mM KCl, 2.3 mM $CaCl_2$, 1.0 mM $MgCl_2$, 3.6 mM $NaHCO_3$, 10 mM glucose, and 5.0 mM HEPES, pH 7.2) according to Mark et al. [10]. H_2O_2 (Sigma) was freshly prepared daily. GSH-ethyl ester (Sigma) and tunicamycin (Sigma) were prepared as 100 × stock solutions in saline. Responses were recorded at room temperature using the whole cell recording configuration of the patch clamp technique with an amplifier (Nihon Kohden, Tokyo, Japan) and data acquisition software (pCLAMP; Axon Instruments, CA, USA). Electrical signals were filtered at 1 kHz. Glass pipettes (2–5 MΩ) were filled with 100 mM CsCl, 2.0 mM $MgCl_2$, 10 mM EGTA, 10 mM HEPES, 15 mM tetraethylammonium chloride, 5 mM Mg-ATP, 20 mM creatine phosphate and 50 units/ml creatine kinase (pH 7.3). Unless otherwise indicated, the recording medium contained the following: 130 mM NaCl, 5.0 mM $CaCl_2$, 2.0 mM $MgCl_2$, 10 mM HEPES, 10 mM glucose, 5.0 mM 4-aminopyridine and 500 nM tetrodotoxin (pH 7.4). Drugs used for the isolation of different Ca^{2+} currents were added to the external solution.

For electrophysiological experiments, cells were carefully selected from cultures according to their morphological characteristics (Fig. 1A, left). The cells were small in size (the average diameter was about 9 μm) and round or oval in shape, consistent with the morphological characteristics of dentate granule cells reported in a previous study [1]. Ca^{2+} currents in the cells were recorded with Cs^+-based pipette solution (Fig. 1A, right). Ca^{2+} currents elicited by depolarizing voltage steps between −50 and +80 mV are shown in Fig. 1B (open circles). Voltage steps were applied for 100 ms from a holding potential of −50 mV. The currents activated around −30 mV, peaked at 0 mV, and reversed around +50 mV. Their kinetics compare well with those of the high voltage-activated (HVA) Ca^{2+} currents reported by Eliot and Johnston [1]. We examined the effects of H_2O_2 on VGCCs in these cells. Pretreatment of the cells with H_2O_2 (1 and 10 μM) for 2 h resulted in a significant increase in the amplitude of the Ca^{2+} current (Fig. 1B,C).

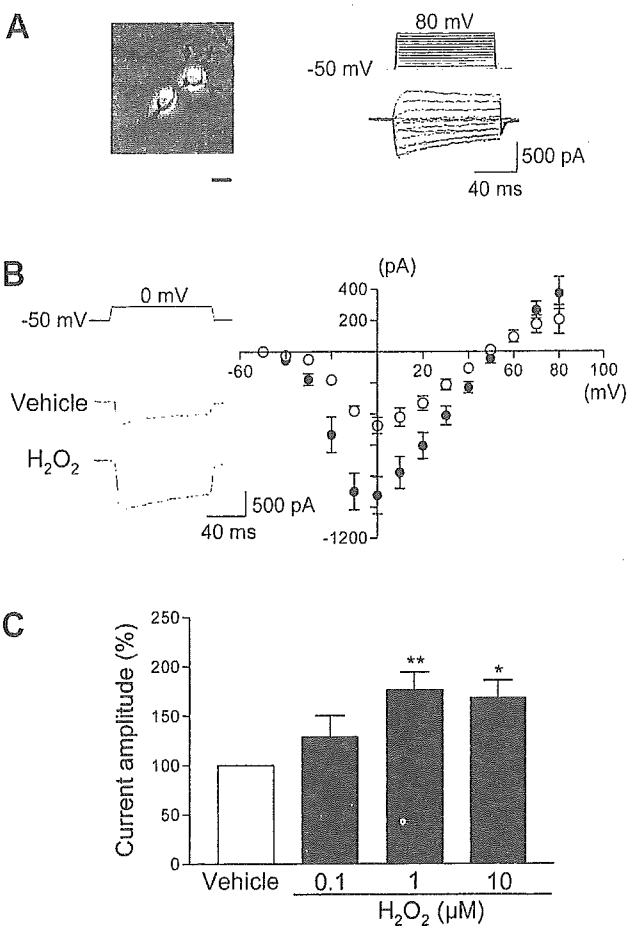

Fig. 1. H_2O_2 enhances whole cell Ca^{2+} current in cultured rat dentate granule cells. (A) Representative photomicrographs of cultured dentate granule cells 7 days after culture (left). Scale bar, 10 μm. Leak-subtracted Ca^{2+} current in a cell elicited by 100 ms step commands from −50 mV (right). (B) Effects of H_2O_2 on the Ca^{2+} current. Representative recordings of the Ca^{2+} current in cells that had been treated for 2 h with either vehicle or 1 μM H_2O_2 (left). Current–voltage relationship of the Ca^{2+} current in vehicle-treated (○, $n = 9$) and H_2O_2-treated (●, $n = 11$) cells (right). (C) Concentration dependency of the effects of H_2O_2 on Ca^{2+} currents. Values are the mean ± SEM of measurements made in four to 21 neurons in at least three separate cultures (**$P < 0.01$, *$P < 0.05$ vs. the vehicle; ANOVA followed by Dunnett's multiple range test).

For higher concentrations of H_2O_2, it was very difficult to record currents after treatment with 20–200 μM H_2O_2 for 2 h, and no living cells were observed at concentrations higher than 200 μM. We used a concentration of 1 μM to analyze the phenomenon in the following experiments because 1 μM H_2O_2 showed a robust and significant effect. The current–voltage relationships in the absence or presence of H_2O_2 showed that the voltage dependence remained unchanged in cells exposed to H_2O_2 (Fig. 1B).

Five types of HVA Ca^{2+} channels (L-, N-, P-, Q- and R-types) have been identified on the basis of their pharmacological and biophysical properties, and selective blockers are available for L-, N-, and P/Q-type Ca^{2+} channels. To determine which types of VGCCs were affected by H_2O_2, we employed blockers of specific channel types. In vehicle-

treated cultures, addition of 2 μM nifedipine (a blocker of L-type Ca^{2+} channels; Sigma), 3 μM ω-conotoxin-GVIA (a blocker of N-type Ca^{2+} channels; Peptides Institute, Osaka, Japan) and 0.3 μM ω-agatoxin-IVA (a blocker of P/Q-type Ca^{2+} channels; Peptides Institute) resulted in a 29.5%, 19.4% and 22.9% decrease in the amplitude of the Ca^{2+} current, respectively (Fig. 2). In H_2O_2-treated neurons, nifedipine caused a 92.8% decrease, ω-conotoxin-GVIA caused a 18.9% decrease, and ω-agatoxin-IVA caused a 22.9% decrease in the Ca^{2+} current amplitude (Fig. 2B), indicating that the H_2O_2-induced enhancement of the Ca^{2+} current was selectively blocked by nifedipine.

Oxidative stress-induced neuronal damage is associated with a decrease of intracellular GSH. It has been shown that a decrease in the GSH level causes the accumulation of intracellular ROS, resulting in Ca^{2+} influx from the extracellular medium [3,4,14]. To investigate whether intracellular GSH prevents H_2O_2-induced enhancement of the Ca^{2+} current, we examined the effects of GSH-ethyl ester, a membrane-permeable form of GSH, on the current. As shown in Fig. 3A, there was no increase in the Ca^{2+} current amplitude when cells were treated with 1 mM GSH-ethyl ester and 1 μM H_2O_2 simultaneously. It has been shown that not only oxidative stress but also endoplasmic reticulum (ER) stress plays a role in neuronal cell death [6–8]. In these

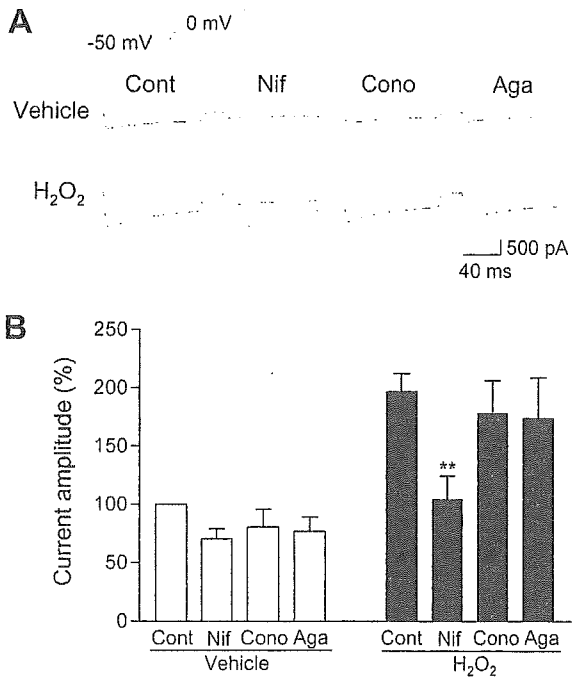

Fig. 2. Effects of Ca^{2+} channel blockers on the amplitude of the Ca^{2+} current in cultured dentate granule cells. (A) Representative recordings of the Ca^{2+} current in the cells. (B) Summarized data of current amplitudes obtained in the absence (Cont) or presence of blockers of specific subtypes of VGCCs (nifedipine, Nif; ω-conotoxin-GVIA, Cono; ω-agatoxin-IVA, Aga) from vehicle-treated (vehicle) and 1 μM H_2O_2-treated (H_2O_2) cells. Values are the mean ± SEM of measurements made in five to 19 neurons in at least three separate cultures (**$P < 0.01$ vs. Cont; ANOVA followed by Dunnett's multiple range test).

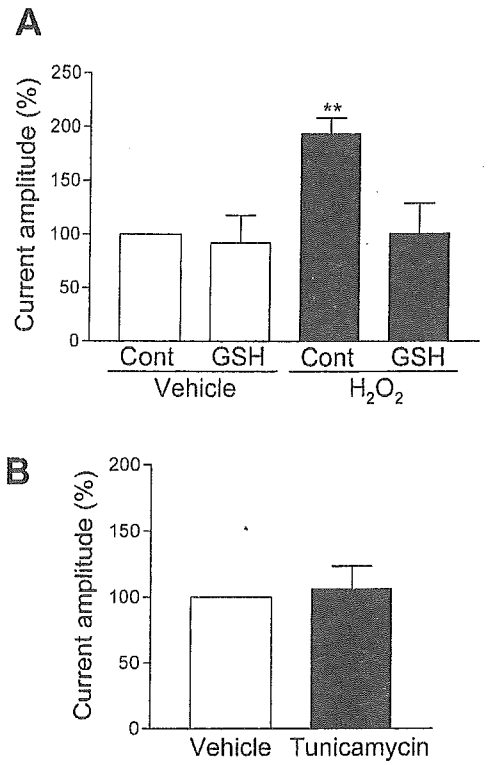

Fig. 3. Effects of simultaneous treatment with GSH and H_2O_2 (A) and tunicamycin (B) on the Ca^{2+} current. Cells were exposed for 2 h to the indicated agents, and whole cell Ca^{2+} current was recorded. (A) GSH-ethyl ester (1 mM) attenuated the H_2O_2 (1 μM)-induced enhancement of the Ca^{2+} current. The values are the means ± SEM of measurements made in five to ten neurons in at least three separate cultures (**$P < 0.01$ vs. the vehicle (Cont); ANOVA followed by Dunnett's multiple range test). (B) Tunicamycin (10 μg/ml) does not affect the Ca^{2+} current. The values are the means ± SEM of measurements made in four neurons in at least three separate cultures.

studies, amyloid β-protein- and tunicamycin (an inhibitor of *N*-glycosylation in the ER)-induced cell death was triggered by ER dysfunction in cultured hippocampal neurons and PC12 cells. We examined the effects of tunicamycin on Ca^{2+} currents in the dentate granule cells. Unlike H_2O_2, tunicamycin (10 μg/ml) induced no current enhancement (Fig. 3B). This result suggests that oxidative stress, but not ER stress, modulates the Ca^{2+} channel activities in these cells.

In the present study, we have demonstrated that pretreatment with H_2O_2 enhances the Ca^{2+} current through L-type Ca^{2+} channels in dentate granule cells. This is the first report to provide direct evidence that H_2O_2 modifies L-type Ca^{2+} channel activity in these cells. The enhancement of the Ca^{2+} current was completely prevented by cotreatment with GSH-ethyl ester. The results are suggestive of involvement of H_2O_2 in modulation of Ca^{2+} channel activities. It has already been reported that H_2O_2 inhibits voltage-gated K^+ channels [12] and $GABA_A$-gated Cl^- channels in rat hippocampal neurons [15]. Our data showing that H_2O_2 did not affect the activity of P/Q-type Ca^{2+} channels are in contrast to a previous report showing that

H_2O_2 enhanced Ca^{2+} currents through P/Q-type Ca^{2+} channels composed of α1A, α2/δ, and β3 subunits at potentials more negative than 0 mV [9]. The discrepancy may be due to differences in experimental conditions. For example, we examined the Ca^{2+} current of cultured dentate granule cells, whereas the previous study measured the current permeating through cloned neuronal Ca^{2+} channels expressed in *Xenopus* oocytes.

The exact mechanisms whereby H_2O_2 selectively enhances the nifedipine-sensitive Ca^{2+} current still remain to be elucidated. Pretreatment with the ER stressor tunicamycin did not affect the Ca^{2+} current. Taken together, these results suggest that oxidative stress may selectively regulate the activity of L-type Ca^{2+} channels in dentate granule cells. Currents through VGCCs are known to be increased by phosphorylation of channel α subunit proteins [18]. H_2O_2 may directly or indirectly increase phosphorylation of the α subunit of L-type Ca^{2+} channels.

Acknowledgements

This work was partly supported by Health and Labour Science Research Grants for Research on Advanced Medical Technology from the Ministry of Health, Labour and Welfare, Japan and a grant-in-aid for scientific research from the Ministry of Education, Culture, Sports, Science, and Technology, Japan (KAKENHI13672319) awarded to K.K.

References

[1] L.S. Eliot, D. Johnston, Multiple components of calcium current in acutely dissociated dentate gyrus granule neurons, J. Neurophysiol. 72 (1994) 762–777.
[2] Y. Ikegaya, N. Nishiyama, N. Matsuki, L-Type Ca^{2+} channel blocker inhibits mossy fiber sprouting and cognitive deficits following pilocarpine seizures in immature mice, Neuroscience 98 (2000) 647–659.
[3] K. Ishige, Q. Chen, Y. Sagara, D. Schubert, The activation of dopamine D4 receptors inhibits oxidative stress-induced nerve cell death, J. Neurosci. 21 (2001) 6069–6076.
[4] K. Ishige, D. Schubert, Y. Sagara, Flavonoids protect neuronal cells from oxidative stress by three distinct mechanisms, Free Radic. Biol. Med. 30 (2001) 433–446.
[5] K. Ito, K. Nakazawa, S. Koizumi, M. Liu, K. Takeuchi, T. Hashimoto, Y. Ohno, K. Inoue, Inhibition by antipsychotic drugs of L-type Ca^{2+} channel current in PC12 cells, Eur. J. Pharmacol. 314 (1996) 143–150.
[6] Y. Ito, M. Arakawa, K. Ishige, H. Fukuda, Comparative study of survival signal withdrawal and hydroxymonenal-induced cell death in cerebellar granule cells, Neurosci. Res. 35 (1999) 321–327.
[7] Y. Ito, Y. Kosuge, T. Sakikubo, K. Horie, N. Ishikawa, N. Obokata, E. Yokoyama, K. Yamashina, M. Yamamoto, H. Saito, M. Arakawa, K. Ishige, Protective effect of S-allyl-L-cysteine, a garlic compound, on amyloid β-protein-induced cell death in nerve growth factor-differentiated PC12 cells, Neurosci. Res. 46 (2003) 119–125.
[8] Y. Kosuge, Y. Koen, K. Ishige, K. Minami, H. Urasawa, H. Saito, Y. Ito, S-Allyl-L-cysteine selectively protects cultured rat hippocampal neurons from amyloid β-protein- and tunicamycin-induced neuronal death, Neuroscience (2004) in press.
[9] A. Li, J. Segui, S.H. Heinemann, T. Hoshi, Oxidation regulates cloned neuronal voltage-dependent Ca^{2+} channels expressed in *Xenopus* oocytes, J. Neurosci. 18 (1998) 6740–6747.
[10] R.J. Mark, M.A. Lovell, W.R. Markesbery, K. Uchida, M.P. Mattson, A role for 4-hydroxynonenal, an aldehydic product of lipid peroxidation, in disruption of ion homeostasis and neuronal death induced by amyloid β-peptide, J. Neurochem. 68 (1997) 255–264.
[11] G.P. Miljanich, J. Ramachandran, Antagonists of neuronal calcium channels: structure, function, and therapeutic implications, Annu. Rev. Pharmacol. Toxicol. 35 (1995) 707–734.
[12] W. Müller, K. Bittner, Differential oxidative modulation of voltage-dependent K^+ currents in rat hippocampal neurons, J. Neurophysiol. 87 (2002) 2990–2995.
[13] W.A. Pedersen, W. Fu, J.N. Keller, W.R. Markesbery, S. Appel, R.G. Smith, E. Kasarskis, M.P. Mattson, Protein modification by the lipid peroxidation product 4-hydroxynonenal in the spinal cords of amyotrophic lateral sclerosis patients, Ann. Neurol. 44 (1998) 819–824.
[14] Y. Sagara, K. Ishige, C. Tsai, P. Maher, Tyrphostins protect neuronal cells from oxidative stress, J. Biol. Chem. 277 (2002) 36204–36215.
[15] R. Sah, F. Galeffi, R. Ahrens, G. Jordan, R.D. Schwartz-Bloom, Modulation of the $GABA_A$-gated chloride channel by reactive oxygen species, J. Neurochem. 80 (2002) 383–391.
[16] B.A. Yankner, Mechanisms of neuronal degeneration in Alzheimer's disease, Neuron 16 (1996) 921–932.
[17] A. Yoritaka, N. Hattori, K. Uchida, M. Tanaka, E.R. Stadtman, Y. Mizuno, Immunohistochemical detection of 4-hydroxynonenal protein adducts in Parkinson disease, Proc. Natl. Acad. Sci. USA 93 (1996) 2696–2701.
[18] G.W. Zamponi, E. Bourinet, D. Nelson, J. Nargeot, T.P. Snutch, Crosstalk between G proteins and protein kinase C mediated by the calcium channel αI subunit, Nature 385 (1997) 442–446.

Available online at www.sciencedirect.com
SCIENCE DIRECT®
ELSEVIER
European Journal of Pharmacology 483 (2004) 29–35
ejp
www.elsevier.com/locate/ejphar

Amino acid substitutions from an indispensable disulfide bond affect $P2X_2$ receptor activation

Ken Nakazawa[a,*], Hiloe Ojima[a,b], Reiko Ishii-Nozawa[b], Koichi Takeuchi[b], Yasuo Ohno[c]

[a] *Cellular and Molecular Pharmacology Section, Division of Pharmacology, National Institute of Health Sciences, 1-18-1 Kamiyoga, Setagaya, Tokyo 158-8501, Japan*
[b] *Department of Clinical Pharmacology, Meiji Pharmaceutical University, Kiyose, Tokyo 204-8588, Japan*
[c] *Division of Pharmacology, National Institute of Health Sciences, 1-18-1 Kamiyoga, Setagaya, Tokyo 158-8501, Japan*

Received 17 July 2003; received in revised form 2 October 2003; accepted 7 October 2003

Abstract

The roles of six amino acid residues downward from an extracellular disulfide bond involving Cys^{224} in rat $P2X_2$ receptor were examined. When Cys^{224} or Pro^{225} was replaced with alanine, the responsiveness to ATP was lost. When Ile^{226} was replaced with other hydrophobic amino acids, the responsiveness to ATP was reduced or abolished. When Phe^{227} was replaced with leucine or isoleucine, the responsiveness to ATP was abolished. The responsiveness to ATP was moderately decreased with the alanine-substitution for Arg^{228} and it was markedly decreased with the alanine-substitution for Leu^{229}. As for the alanine-substitution for Gly^{230}, the sensitivity was changed, but the maximal response to ATP was not reduced. The results suggested that a precise structure is required for amino acid residues close to the disulfide bond and, in general, the amino acid residues at odd number positions and those closer to the disulfide bond are more influential to the ATP responsiveness.

Keywords: P2X receptor; ATP; Site-directed mutagenesis; *Xenopus* oocyte; Membrane current

1. Introduction

P2X receptors are ion channel-forming membrane proteins that are activated by extracellular ATP (see reviews, Khakh, 2001; North, 2002). One functional ion channel is presumably formed by three homogenous subunits. Each subunit has two transmembrane regions (TM1 and TM2) and a long extracellular loop (E1) between them. Basic amino acid residues near the outer mouth of the channel pore formed by TM1 and TM2 appear to serve as a part of the binding pocket of ATP molecules (Ennion et al., 2000; Jiang et al., 2000). In addition to these basic residues, amino acid residues in E1 apart from the channel pore have been shown to affect the channel activation by ATP. $P2X_2$ receptor did not respond to ATP when Gly^{247} in E1 was replaced with alanine (Nakazawa and Ohno, 1999). The sensitivity to ATP was reduced when Gly^{248} was replaced with valine and the responsiveness was lost when the residue was replaced with leucine (Nakazawa et al., 2002). The replacement of Trp^{256} with other amino acid residues except for tyrosine also resulted in the loss of responsiveness (Nakazawa et al., 2002). These results suggest that the structure around these positions should be precisely maintained for the channel activation by ATP. Recently, the pairs of cysteines that form disulfide bonds have been identified for $P2X_1$ (Ennion and Evans, 2002) and $P2X_2$ (Clyne et al., 2002) receptors. Among these cysteines, the structure formed by Cys^{224} through a disulfide bond with Cys^{214} appears to be critical because the replacement of this residue with alanine was non-functional (Clyne et al., 2002). Cys^{227} in $P2X_1$, which corresponds to Cys^{224} in $P2X_2$ (see Fig. 1), may also play an indispensable role in the formation of such a structure because its alanine substitution resulted in about 50-fold reduction in the sensitivity to ATP (Ennion and Evans, 2002). In the present study, we examined the roles of amino acid residues following Cys^{224} in $P2X_2$ receptor to understand

* Corresponding author. Tel.: +81-3-3700-9704; fax: +81-3-3707-6950.
E-mail address: nakazawa@nihs.go.jp (K. Nakazawa).

0014-2999/$ - see front matter © 2003 Elsevier B.V. All rights reserved.
doi:10.1016/j.ejphar.2003.10.026

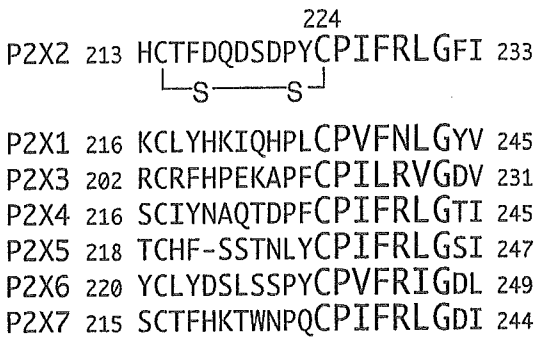

Fig. 1. Amino acid sequence near Cys^{224} in the extracellular loop of $P2X_2$ receptor and corresponding sequences of P2X receptor subclasses. Amino acid residues targeted for site-directed mutagenesis and those in the equal positions were shown as the larger characters. Cys^{224} forms a disulfide bond with Cys^{214}.

structural requirements for the channel activation in this region.

2. Materials and methods

2.1. Oocyte expression and membrane current measurements

The expression of cloned and mutant $P2X_2$ receptor and the recordings of ionic current through the channels were performed according to our previous report (Nakazawa et al., 1998). Briefly, $P2X_2$ receptor mutants were constructed from the cloned $P2X_2$ receptor (Brake et al., 1994) by site-directed mutagenesis. Amino acid residues targeted for mutagenesis were shown in Fig. 1. The wild-type and the mutant channels were expressed in *Xenopus* oocytes for a 4-day incubation at 18 °C and the oocytes were served for membrane current measurements. Oocytes were bathed in ND96 solution containing (in mM) NaCl 96, KCl 2, $CaCl_2$ 1.8, $MgCl_2$ 1, HEPES 5 (pH 7.5 with NaOH). ATP (adenosine 5′ -triphosphate disodium salt; Sigma, St. Louis, MO, USA) was applied by superfusion for about 6 s with a regular interval of 1 min.

2.2. Immunoblotting analysis

The expression of channel protein was confirmed by immunoblotting analysis. Crude membrane fractions were prepared from oocytes (20 oocytes for the wild-type channel and each mutant) according to Newbolt et al. (1998) with minor modifications. Oocytes were suspended in a 50 × stock of a protease and phosphatase inhibitor cocktail (Sigma, general use; 1 bottle for 100 ml effective solution) diluted in a buffer containing 20 mM Tris–HCl, 2 mM EDTA (disodium salt), 0.5 mM EGTA and 320 mM sucrose by pipetting. The homogenate was horizontally shaken at 100 rpm for 15 min at 4 °C and then centrifuged at 14,000 rpm for 2 min. The supernatants were analyzed by SDS-PAGE gel electrophoresis and immunoblotting. By using $P2X_2$ receptor antibodies (Oncogene, Boston, MA, USA) and anti-rabbit Ig, horseradish peroxidase-linked whole antibody (from donkey; Amersham, Little Chalfont, England), correct channel expression was detected as a 65-kDa band.

2.3. Data analysis

Parameters for ATP sensitivity (EC_{50}, pD_2 and Hill coefficient) were obtained from current responses using the following equation:

$$E = E_{max}A^n/[A^n + (EC_{50})^n], \quad (1)$$

where E is an effect (current response), E_{max} is an maximal response, A is ATP concentration, EC_{50} is concentration required for a half-maximal effect and n is a Hill coefficient (slope factor). When EC_{50} and n were calculated from ATP concentrations used and obtained current responses, Eq. (1) was transformed to:

$$\log[E/(E_{max} - E)] = n(\log A - \log EC_{50}), \quad (2)$$

and linear regression was made using Microsoft® Excel X. pD_2 values were negative logarithm of EC_{50} values. When experimental data were fitted by a two binding-site model, the fraction of one binding-site (f) and that of the other binding-site ($1-f$) were introduced. The effect mediated through each binding-site was calculated from Eq. (1) and the fraction (f or $1-f$), and the sum of these effects was obtained.

3. Results

3.1. Amino acid substitutions and ATP responsiveness

Cys^{224} and neighboring Pro^{225} are completely conserved among seven subclasses of P2X receptors (Fig. 1; Soto et al., 1997). Fig. 2 shows concentration–response relationship for ATP-evoked current recorded from oocytes expressing the wild-type $P2X_2$ receptor and the Cys^{224}- or Pro^{225}-to-alanine-substituted mutants (C224A or P225A, respectively). C224A exhibited no current response to ATP, as has been reported by Clyne et al. (2002). P225A also failed to respond to ATP. To examine the effects of amino acid residues succeeding to Pro^{225}, we first constructed deletion mutants. When three residues next to Pro^{225} (Ile^{226}, Phe^{227} and Arg^{228}) were deleted, the responsiveness to ATP was lost. Deletion of the former two or even Ile^{226} alone also resulted in the loss of the responsiveness. The preliminary results suggest that these amino acid residues also appeared to be essential. Thus, instead of deletion, we introduced amino acid substitutions to these residues in a one-by-one manner.

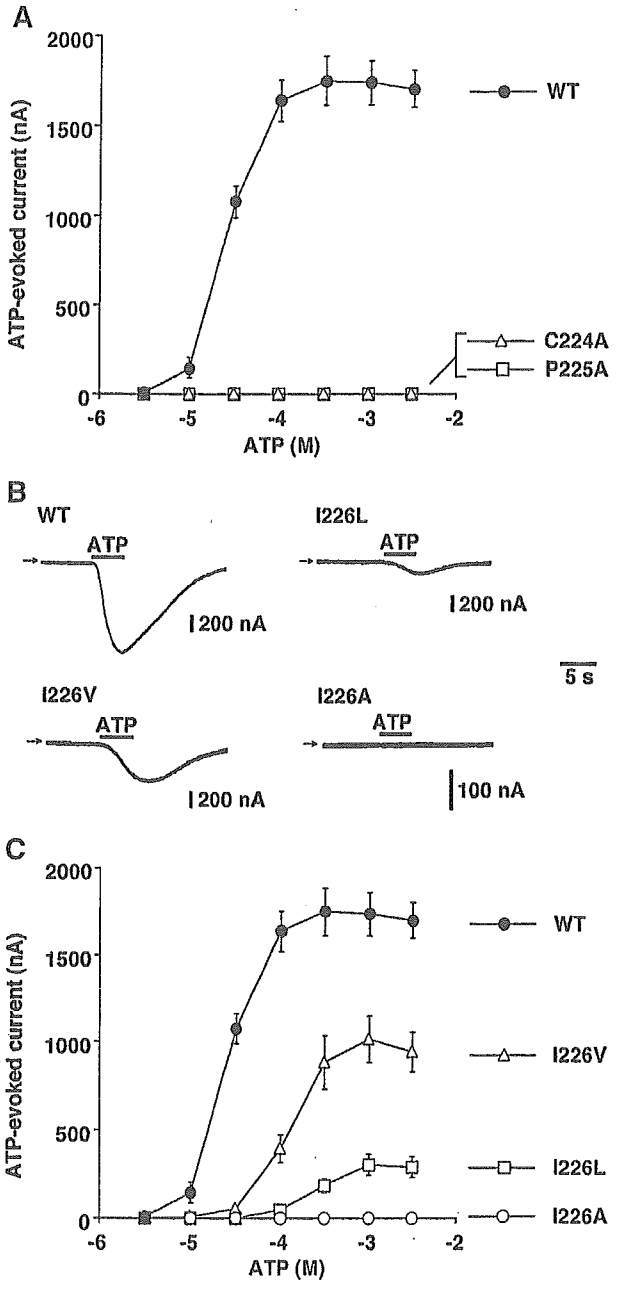

Fig. 2. (A) Disappearance of current responses to ATP by the replacement of Cys^{224} or Pro^{225} with alanine (C224A or P225A). Peak amplitude of currents activated by ATP at −50 mV was plotted against ATP concentrations. Each symbol and bar represent mean and S.E. obtained from five to eight oocytes. In contrast to current responses in oocytes expressing the wild-type channel (WT), no response was observed in those expressing the mutant channels. (B) Currents activated by 30 μM ATP in oocytes expressing the wild-type (WT) and Ile^{226}-to-leucine (I226L), -valine (I226V) and -alanine (I226A)-substituted mutant channels. The oocytes were held at −50 mV. Arrows indicate zero current levels. (C) Concentration–response relationship for the wild-type and Ile^{226}-replaced channels. The current responses were obtained as shown in B. The concentration–response relationship for the wild-type channel (WT) was also shown for comparison. Each symbol and bar represent mean and S.E. obtained from five to eight oocytes.

Ile^{226} was replaced with hydrophobic amino acid residues because this position was occupied by isoleucine or valine in seven P2X receptor subclasses (Fig. 1). Fig. 2B shows current responses to 100 μM ATP in oocytes expressing the wild-type and the mutant channels. When substituted with leucine, which has a volume similar to that of isoleucine (Chothia, 1975), the ATP-evoked current was markedly reduced (Fig. 2B,C; I226L). When substituted with valine, a smaller hydrophobic residue, the reduction of the current

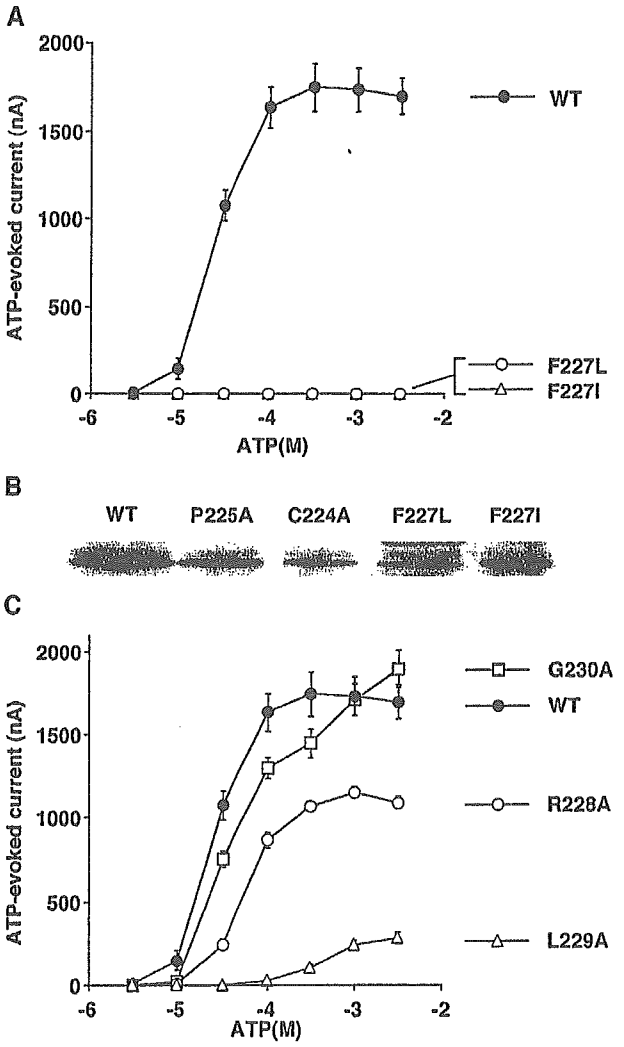

Fig. 3. (A) Disappearance of current responses to ATP by the replacement of Phe^{227} with leucine (F227L) or isoleucine (F227I). Data obtained from five to eight oocytes were shown as in Fig. 2A. (B) Immunoblotting analysis using anti-$P2X_2$ receptor antibody. A section corresponding to $P2X_2$ receptor protein (about 65 kDa) was shown to compare the expression in membrane fractions prepared from the oocytes injected with the wild-type channel (WT) and four non-ATP responsive mutants shown in Fig. 2A (C224A and P225A) and A of this figure (F227L and F227I). (C) Concentration–response relationship for the wild-type and Arg^{228}-(R228A), Leu^{229}- (L229A) and Gly^{230}-to-alanine-substituted mutants. The concentration–response relationship for the wild-type channel (WT) was also shown for comparison. Data obtained from five to eight oocytes were shown as in Fig. 2A.

was less remarkable than in the case of the leucine-substitution (Fig. 2B,C; I226V). When substituted with alanine, a hydrophobic residue smaller than valine, the current responsiveness to ATP was abolished (Fig. 2B,C; I226A).

Phe^{227}, a residue succeeding to Ile^{226}, is conserved among six of seven P2X receptor subclasses (Fig. 1). In the remaining subclass ($P2X_3$), leucine is present instead of phenylalanine. When Phe^{227} was replaced with leucine, the current response to ATP disappeared (Fig. 3A; F227L). The current response has also disappeared when replaced with isoleucine (Fig. 3A; F227I). The disappearance of the current response may not be due to non-expression of receptor protein because the protein expression of F227L or F227I was confirmed by immunoblotting analysis (Fig. 3B). The protein expression was also confirmed for the C224A, P225A (Fig. 3B) or I226A (not shown).

Three residues succeeding to Phe^{227} were alanine-substituted (Fig. 3C). The current response to ATP was reduced to about 60% when Arg^{228} was replaced with alanine (R228A). The current response was, however, much reduced (to about 20%) when Leu^{229} was replaced with alanine (L229A). As for the replacement of Gly^{230}, the maximal current response was comparable to that with the wild-type channel (G230A).

3.2. Sensitivities to ATP

To compare the sensitivity to ATP, the concentration–response data were normalized to the maximal response (Fig. 4). Theoretical curves were fitted to the normalized data (see Section 2), and EC_{50} values and Hill coefficients were determined. For the wild-type channel, the EC_{50} value was 29 μM and the Hill coefficient was 2.3. Ile^{226}-, Arg^{228}- and Leu^{229}-substituted mutants exhibited lower sensitivities to ATP than the wild-type channel did (Fig. 4A–C), and the order of the sensitivities was R228A>I226V ≈ I226L>L229A. Hill coefficients for these mutants (varying from 1.7 to 2.6) were similar to that for the wild-type channel. When the curve fitting was applied to the data with G230A, the Hill coefficient as well as the ATP-sensitivity was lower than those for the wild-type channel (Fig. 4D, solid curve). The data points in Fig. 4D were, however, not well fitted to the solid curve. In fact, a regression coefficient of the fitting for the G230A

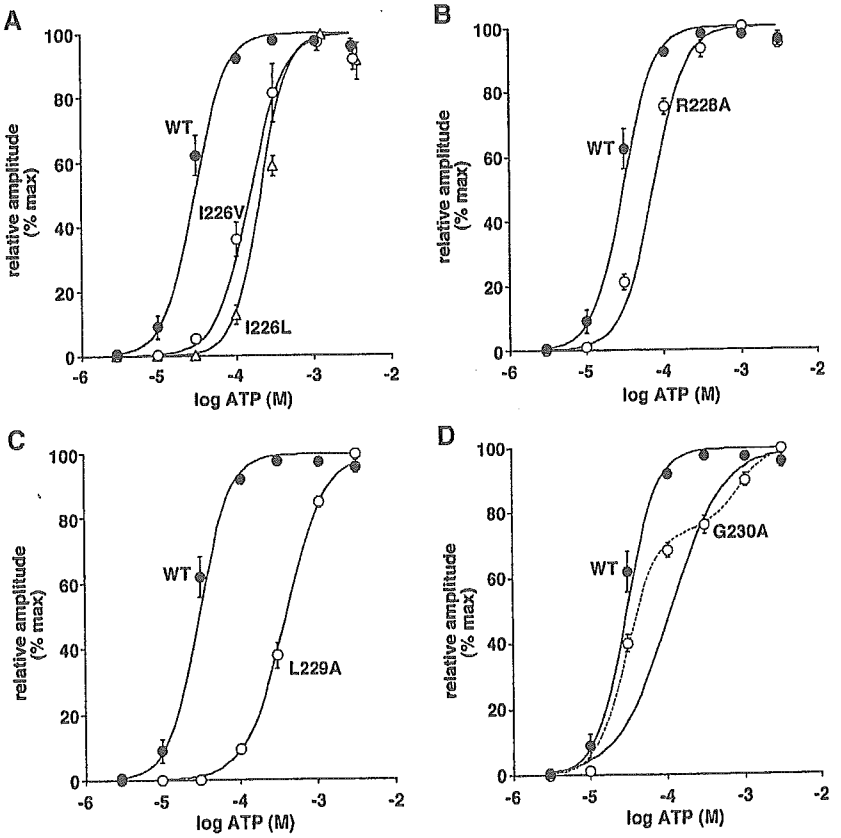

Fig. 4. (A–C) Curve-fittings to concentration–response data for the wild-type and the mutant channels. Current responses to ATP were normalized to maximal responses in individual oocytes and mean values were plotted against ATP concentrations. A curve was fitted to data assuming a homogenous binding-site for each channel type as shown in Section 2. Bars are S.E. Parameters calculated and used for fittings are: EC_{50} (in μM); 29 (WT), 151 (I226V), 202 (I226L), 72 (R228A), 379 (L229A), 108 (G230A); Hill coefficient; 2.3 (WT), 2.0 (I226V), 2.6 (I226L), 2.1 (R228A), 1.7 (L229A), 1.3 (G230A). (D) Curve-fittings to concentration–response data for G230A mutants. The data and were shown and the solid curve with an EC_{50} value of 108 μM and a Hill coefficient of 1.3 was fitted to the data as in A–C. For the broken curve, it was constructed assuming 75% of binding sites are equivalent to the wild-type receptor and the remaining 25% of binding sites have a lower affinity (EC_{50}; 800 μM) and the same slope (Hill coefficient; 2.3).